CESIUM MAGNETOMETER DEVELOPMENT

James H. Simpson

Singer Company

Prepared for:

Office of Naval Research

4 October 1972

Research Center

AD753060

Report KD-72-87

TECHNICAL REPORT

FOR PERIOD 4 October 1971 TO 3 October 1972

ON

CESIUM MAGNETOMETER DEVELOPMENT

Prepared for:

DEPARTMENT OF NAVY
OFFICE OF NAVAL RESEARCH
WASHINGTON, D.C.

Under
Contract No. N00014-72-C-0087

Report Prepared by:

JAMES H. SIMPSON

October 4, 1972

APPROVED FOR PUBLIC RELEASE, DISTRIBUTION UNLIMITED

SINGER
KEARFOTT DIVISION

Security Classification

DOCUMENT CONTROL DATA - R & D

Security classification of title, body of abstract and indexing annotation must be entered when the overall report is classified)

1 ORIGINATING ACTIVITY (Corporate author) The Singer Co., Kearfott Division Pleasantville, N.Y. 10570	2a. REPORT SECURITY CLASSIFICATION UNCLASSIFIED 2b. GROUP

3 REPORT TITLE

Cesium Magnetometer Development

4 DESCRIPTIVE NOTES (Type of report and inclusive dates)

Technical Report 4 October 1971 to 3 October 1972

5 AUTHOR(S) (First name, middle initial, last name)

James H. Simpson

6 REPORT DATE 4 October 1972	7a TOTAL NO OF PAGES ~~59~~ 66	7b NO OF REFS 19
8a CONTRACT OR GRANT NO N00014-72-C-0087 b PROJECT NO c d	9a ORIGINATOR'S REPORT NUMBER(S) KD-72-87 9b OTHER REPORT NO(S) (Any other numbers that may be assigned this report)	

10 DISTRIBUTION STATEMENT

Approved for public release, distribution unlimited

11 SUPPLEMENTARY NOTES	12 SPONSORING MILITARY ACTIVITY Department of the Navy Office of Naval Research Arlington, Virginia 22217

13 ABSTRACT

The feasibility of building a two-cell cesium gradient magnetometer with a sensitivity of 0.1 mγ has been demonstrated. The theory of operation of an optically pumped magnetometer has been used to determine the cell performance required to obtain a sensitivity of 0.1 mγ. A cell development program has resulted in buffered cesium cells which exhibited signal-to-noise ratios of 100 dB (1 Hz) and traverse relaxation times of about 7 ms. Unbuffered cells with signal-to-noise ratios of 85 dB and relaxation times of about 13 ms were also made. These cell performances are near, or above the theoretical requirements. Tests of a single sensor magnetometer showed a sensitivity of 1 mγ for a 90 Hz magnetic field. The 90 Hz perturbation was applied along the dc field direction and detected as an FM sideband of the resonance frequency observed as the output of a self-oscillating magnetometer. The theory predicts a factor of 10 increase in sensitivity as the frequency decreases to 5 Hz, but this could not be tested because the ambient magnetic noise was too strong in this frequency region. To the extent that fluctuations in the ambient field are the same at both cells in the gradient configuration, this limitation will be eliminated.

DD FORM 1 NOV 65 1473

I-a

Security Classification

14 KEY WORDS	LINK A		LINK B		LINK C	
	ROLE	WT	ROLE	WT	ROLE	WT
Magnetometer						
Gradient Magnetometer						
Magnetic Resonance						
Spin Generator						
Optical Pumping						
Cesium						

FOREWORD

This report describes preliminary investigations for the design of a microgradient magnetometer. The report was prepared by The Singer Co., Kearfott Div., Pleasantville, New York on ONR Contract N00014-72-C-0087.

The studies began in October 1971 and concluded in October 1972. The investigations were conducted under the supervision of I. A. Greenwood, Manager of the Physics Department and under the direction of Dr. J. H. Simpson, Principal Scientist in the Physics Department. The principal contributors were D. I. Shernoff and Dr. D. S. Bayley. Professors R. Novick and W. Happer of Columbia University served as consultants on optical pumping.

The sections of this report concerned with cell fabrication were authored by D. I. Shernoff.

TABLE OF CONTENTS

TABLE OF CONTENTS (continued)

LIST OF ILLUSTRATIONS

SECTION 1

INTRODUCTION

1.1 PURPOSE OF THE PROGRAM

The purpose of this program is to develop a magnetic resonance gradient magnetometer that is of higher sensitivity than those now available. Such an instrument would provide improved range and signature determining capabilities as compared with single sensor instruments. The approach that is taken is an outgrowth of a series of investigations concerned with both the fundamentals of optical pumping magnetic resonance and with other applications of this phenomenon.

The portion of the investigation described in this report is concerned with the development of experimental techniques and supporting theory that will allow the construction of a gradient magnetometer with a differential sensitivity of 0.1 milligamma. This would correspond to a gradient sensitivity of 0.1 mγ/ft if the two sensors are spaced one foot apart.

1.2 SUMMARY OF THE TECHNICAL PROBLEM

1.2.1 Single-Sensor Magnetometer

An optically-pumped, magnetic-resonance magnetometer determines the magnitude of the magnetic field by a measurement of the resonance frequency of the atoms in the sensor cell. Typically the resonance material is metastable helium, rubidium, or cesium. Mercury also has been used. Typical sensitivity of the single sensor magnetometers is about 0.1 to 0.01 gamma. (Refs. 1, 2).

Although additional improvement can be made in single sensor devices, the greater sensitivity cannot in general be fully utilized

in the ambient earth's magnetic field because of the random and quasi-random fluctuations in the earth's field. Those components at or near 1 Hz may have amplitudes up to 1 γ. Lower frequency components may be more than an order of magnitude higher (Ref. 3) and are attributed to currents in the earth's ionosphere and magnetosphere.

In addition there is geological noise, which originates from the motion of the sensor through the spatially varying magnetic field of the earth. These variations are caused by the differing magnetic properties of the earth's crust.

A single resonance cell unit will also possess maneuver error, in that the magnetic sensor behaves like a gyro: its frequency is constant only in a non-rotating framework. Rotation of the sensor cannot be distinguished from a field change.

In addition the sensitivity of a single cell sensor is a function of the signal-to-noise of the detected magnetic resonance signal. Other sources of random variation in magnetometer output include the orientation of the instrument in the magnetic field and the intensity and spectral distribution of the optical pumping light beams.

1.2.2 Gradient Measuring Devices

Gradients in the earth's magnetic field can be determined from simultaneous measurement of the field at two points separated by a fixed distance. A single-sensor magnetometer at each point would provide the means for observation. One advantage of gradient operation is that fluctuations in the magnetic field originating from distant sources are approximately the same at both sensors and do not produce an output. The gradient in the magnetic field produced by a source decreases as the fourth power

of the distance while the magnitude of the field decreases only as the third power of the distance. This same property provides an indication of range.

With a very sensitive pair of cells, the base line between the sensors can be shortened and very small changes in gradient detected. With the sensors close together the conditions of operation in each unit can be made so nearly the same that perturbations in performance induced by changes in experimental parameters will be the same at both cells and cancel. That is, most perturbations to the sensors can be reduced to very small differential effects. The same would apply to gyroscopic effects.

A distinction between the various magnetic gradient sensors should be noted, particularly if considering incorporating the output in some systems application. Each magnetic resonance sensor ideally measures the magnitude of the earth's field $|\vec{H}|$ at its position. (Orientation effects are second order or lower.) A gradient measurement using magnetic resonance sensors measures one of the three components of the total gradient $\vec{\nabla}|\vec{H}|$.

Gradient measuring devices which use superconducting sensors determine the gradient of the components of the magnetic field. Takken (Ref. 4) most clearly indicates this difference between the two types of instruments and shows the latter to be measuring the components of the dyadic $\vec{\nabla}\vec{H}$. Dyadic measuring devices are extremely sensitive to torsion or bending which produces relative angular motion between the two sensors. An instrument measuring $\vec{\nabla}|\vec{H}|$ will not be so sensitive to the changes in the relative orientation of the two sensors.

1.3 SUMMARY OF ACTIVITIES

The experimental and analytical work performed during this program was directed toward the demonstration of experimental techniques

required for designing a gradient magnetometer having a useful differential sensitivity of 0.1 milligamma or better.

The analytical work was concerned with the development and application of a theory describing the effects of signal-to-noise, random phase shifts, and light-induced frequency shifts on the sensitivity of a single-cell sensor. From the theory of phase perturbations in a spin generator, specifications were obtained for the parameters signal-to-noise ratio and transverse relaxation time.

A new approach has been found for calculating the perturbations due to the light induced frequency shift. In the new formulation the results are in an analytic form thus greatly reducing the requirements for extensive numerical analysis.

The experimental work was directed toward the achievement of the values for the experimental parameters specified by the analytical work and toward the demonstration of single-sensor magnetometer performance approaching the value of 0.1 mγ. Apparatus was assembled for the dual purposes of measuring the sensor cell parameters and for operation as a magnetometer. Another part of the experimental program was concerned with the development of techniques for fabrication of sensor cells with the desired characteristics.

The laboratory apparatus provides for the optical, magnetic and electronic components required for driving and detecting the magnetic resonance signals. The sensitive portions of the apparatus were enclosed in a triple-layer magnetic shield in order to attenuate the ac and dc components of the ambient magnetic field. The photodetector and associated circuitry were chosen to provide maximum signal-to-noise ratio. The design was accomplished using non-magnetic components inside the shielded enclosure.

In the cell development program, uncoated cells with different buffer gas components and pressures were first made. Then wax-coated, vacuum cells were made using a variety of techniques and materials.

Buffered cesium resonance cells were constructed that exhibited signal-to-noise ratios of 100 dB (1 Hz) and relaxation times of about 7 msec. The equivalent values for unbuffered cells are signal-to-noise ratios of over 85 dB* and relaxation times of about 13 msec. These values are within the limits required for a differential sensitivity of 0.1 mγ.

As confirmation of the validity of the analysis relating performance capability to signal-to-noise ratio and transverse relaxation time,tthe apparatus was operated in the self-oscillating magnetometer mode and its sensitivity determined by measuring the known amplitude of weak perturbing magnetic fields. Magnetic field changes of 20 mγ at a frequency of 90 Hz were introduced. The magnetometer measured this change as 18.0 ± 2.4 mγ, thus demonstrating with a single cell magnetometer a sensitivity within almost an order of magnitude of the ultimate differential sensitivity of 0.1 mγ. Fluctuations of the ambient field even as attenuated by the magnetic shield were so large at lower frequencies that weak perturbing signals were masked by the background.

The theory of this mode of magnetometer operation allows one to extrapolate from the 2 mγ performance at 90 Hz to a sensitivity of 0.2 mγ at 10 Hz with the same single sensor magnetometer.

* In the remainder of this report the signal-to-noise ratio in dB refers to the ratio of signal power to noise power per Hz unless otherwise designated.

SECTION II

2.0 REVIEW OF THE BASIC DESIGN OF THE GRADIENT MAGNETOMETER

The basic design of the gradient magnetometer is shown in Figure 2-1. Two identical optically-pumped magnetic-resonance cells are separated by a distance that will probably be about 0.5 meters. From the work performed on this program, the most likely material for use in the sensors is cesium-133 although the use of rubidium-85 or rubidium-87 is not completely ruled out.

In this design the light for the two pumping beams is obtained from a single common beam. It is filtered to pass the D_1 component for efficient optical pumping. The division of the unpolarized beam into its two components of orthogonal polarization can be accomplished by means of a beam splitting polarizer, which can be a stack of thin glass plates mounted at the Brewster angle or one of various types of split, crystal prisms. Obtaining the two beams from a common beam ensures that the intensity and spectral fluctuations in the two beams remain identical. Two mirrors then direct the beams toward the cells. Prior to entering the cell each beam is circularly polarized in order to promote the optical pumping process.

A second light source provides the readout beams. After collimation the beam passes through a D_1 filter and like the pumping beam is split into its two orthogonal senses of polarization. If Faraday readout is to be used on the resonance, each beam is linearly polarized before traversing the cell. An analyzer in each of the transmitted beams converts the modulation in angle of polarization introduced by the resonance atoms to amplitude modulation which is then detected by means of a photodetector.

If Dehmelt readout (Ref. 5) is used, each crossbeam is circularly polarized before entering the cell. No analyzer is required in front of the photodetector.

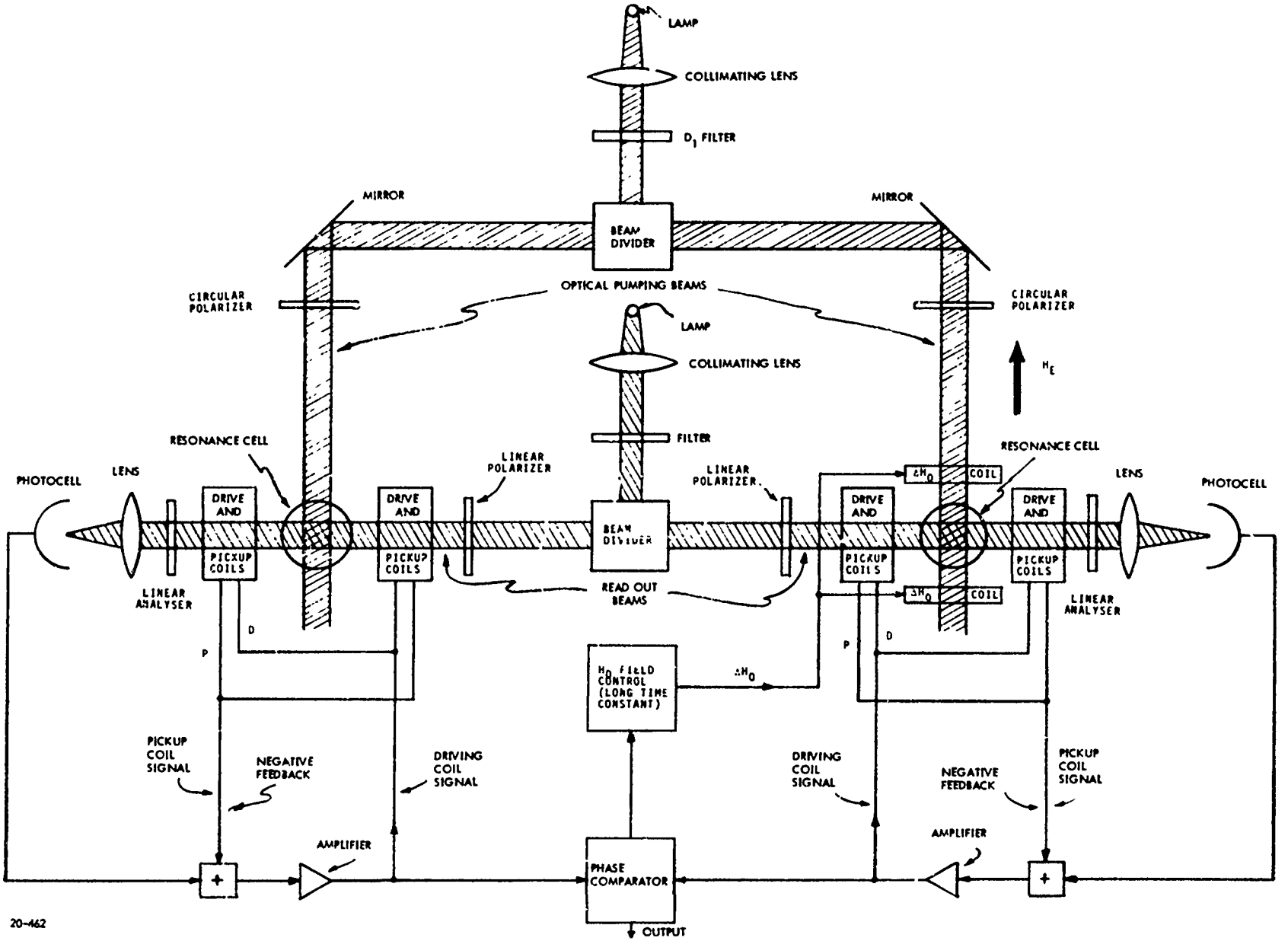

PROPOSED MICROGRADIENT MAGNETOMETER
FIGURE 2-1

Each resonance cell is placed between a pair of rf driving coils which are oriented to be coaxial with the readout beam. This ensures that the phase shift in the spin generator loop will not be affected significantly by changes in direction of the earth's magnetic field.

Spin generator action is obtained by using the amplified output from each photocell to drive the rf coils that produce the H_1 magnetic field. A very flat frequency response and hence a very small electrical phase shift are obtained by using a negative feedback amplifier with a high open-loop gain.

The use of a readout beam parallel to the H_1 magnetic field introduces a 90° geometrical and frequency independent phase shift between the field and the output of the photocell. This is compensated by using the voltage induced in a pair of pickup coils to energize the high impedance negative feedback path to the amplifier. These coils are wound on the same forms as the rf driving coils, and the resulting close magnetic coupling minimizes phase shifts caused by eddy currents induced in nearby conductors. Phase shifts introduced by the close capacitive coupling can be made very small by proper choice of the turns and resistance ratios of the two sets of coils. This arrangement has been tested in the nuclear gyro and performs as predicted. (Ref. 6)

Each spin generator feeds the phase comparator whose principal output is a signal proportional to the phase difference accumulated over a preset observation time t. This, in turn, is proportional to the integral over this time of the difference ΔH in the magnetic fields that determine the frequency of each spin generator.

A second and continuous output from the phase comparator is fed to the ΔH_o field control which contains a suitable amplifier and

smoothing circuit with a long time constant. The amplified and filtered signal energizes the ΔH_o coil which changes the frequency of one spin generator so as to null the average value of the phase difference over the long smoothing time.

The initial current through the ΔH_o coil can be adjusted to cancel the effect of any constant difference in the earth's magnetic field at the two spin generators. The smoothing and observation times can be set to minimize the effect of fluctuations in the earth's differential field on the sensitivity of the magnetometer to an input signal of a given signature. The time constant of the smoothing circuit would be of the order of ten to one hundred times the time constant of the signal circuit. The signal processing method shown in Figure 2-1 indicates a mode of function and not an optimization to match the statistical or non-statistical nature of the signals to be detected.

2.1 INFLUENCE OF SIGNAL-TO-NOISE RATIO

As pointed out in Section 2.0, the effects of slow fluctuations in the magnitude of the earth's gradient magnetic field are to be minimized by the smoothing circuit on the output of the phase comparator and the ΔH_o correction coil. This section will consider the noise generated by fluctuations in the production rate of photoelectrons in the photodetector and the influence of this noise on the performance of the gradient magnetometer. The noise has two effects, the limitation of ability to determine the phase of the oscillation and the perturbation of the phase of the spin generator oscillations. The fluctuation in number of photoelectrons constitutes the major source of noise.

Consider first the limitation of ability to determine phase. At the output of the phase comparator the corresponding noise voltage (amplitude) is taken to be in quadrature with the signal voltage S. This will introduce an uncertainty $\Delta\phi_1$ in the phase measurement given by

$$\Delta\phi_1 \approx N/S. \qquad (2\text{-}1)$$

Since shot noise in the photomultiplier dominates all other noise sources in the spin generator feedback path, the signal and noise can in practice be taken as that measured at the photocell. The signal can then be defined as the number S of photoelectrons emitted during the observation time, t, i.e.,

$$S = QP_M t, \tag{2-2}$$

where Q is the quantum efficiency of the photocell and P_M is the average photon arrival rate corresponding to the amplitude of the modulation of the readout beam.

Since the average intensity of the readout beam is larger than the amplitude of the intensity modulation, the noise will be the rms value of the fluctuations in the photoelectron count originating from this unmodulated portion of the readout light. Hence the noise N is

$$N = (QP_A t)^{\frac{1}{2}}, \tag{2-3}$$

where P_A is the average rate of arrival of the readout beam photons.

The limitation to which the phase can be measured is obtained by substitution of equation (2-2) and (2-3) in (2-1),

$$\Delta\phi_1 = P_M^{-1}(P_A/Qt)^{\frac{1}{2}}. \tag{2-4}$$

The second effect of the noise, the perturbation of the phase of the oscillation, can be estimated from the theory of noise in a classical oscillator (Ref. 7). In one approach to this theory, the phase is considered to be measured once each relaxation time τ and this information used to start the precession once again. The phase error introduced by a measurement after one relaxation

time τ, $\Delta\phi(\tau)$ can be obtained from equation 2-4, and is

$$\Delta\phi(\tau) = P_M^{-1}(P_A/Qt)^{\frac{1}{2}}. \tag{2-5}$$

In a time t, there will be (t/τ) independent measurements, thus the total phase error will be

$$\Delta\phi_2 = (P_M\tau)^{-1}(P_A t/Q)^{\frac{1}{2}}. \tag{2-6}$$

Assuming the errors $\Delta\phi_1$ and $\Delta\phi_2$ to be independent, the total error is

$$\Delta\phi = \frac{N}{S}_1 t^{-\frac{1}{2}} \left(1 + \frac{t^2}{\tau^2}\right)^{\frac{1}{2}} \tag{2-7}$$

where $(N/S)_1$ is $(P_A/Q)^{\frac{1}{2}}/P_M$ and is just the ratio of amplitudes corresponding to the ratio of signal power to noise power at unit bandwidth.

The total error $\Delta\phi$ will limit the sensitivity of the microgradient magnetometer to a minimum detectable magnetic field difference $\overline{\Delta H}_{min}$ determined by

$$\overline{\Delta H}_{min} = \Delta\phi/(\gamma t), \tag{2-8}$$

where γ is the gyromagnetic ratio and the magnetic field difference is averaged over the preset observation time t for detection of the signal.

The potential performance capabilities of the gradient magnetometer can be described in terms of the experimental parameters and variables by combining equations 2-7 and 2-8 to give,

$$\overline{\Delta H}_{min} = \frac{N}{S}_1 \gamma^{-1} t^{-3/2} \left(1 + \frac{t^2}{\tau^2}\right)^{\frac{1}{2}} \qquad (2\text{-}9)$$

From this relationship, ranges of values for the various parameters can be calculated that correspond to performance capabilities; that is, values of $\overline{\Delta H}_{min}$ that correspond to various values of the variable t, the time of observation. Signal-to-noise ratios were chosen to be in the already attained range: 80 dB, 90 dB, and 100 dB; relaxation times were chosen as 0.01 sec, 0.05 sec, and 0.10 sec, and $\overline{\Delta H}_{min}$ calculated for observation times such that $\overline{\Delta H}_{min}$ was of the order of 0.1 milligamma or better. The results of these calculations are summarized in Figure 2-2 where the values of $\overline{\Delta H}_{min}$ as a function of t are plotted for given combinations of signal-to-noise and relaxation time. For most of the range of values these functions are straight lines on a log-log plot. All curves corresponding to a signal-to-noise ratio of 80 dB are shown as a solid line, those corresponding to 90 dB are shown as a dashed line, and those corresponding to 100 dB are shown as alternated dashes and dots. For example, assuming a signal-to-noise ratio of 90 dB and a relaxation time of .01 sec, an observation time of two seconds is required for detecting a field change of 10^{-9} gauss. The two curves shown with dash and two dots correspond to performance calculated for observed experimental parameters.

To convert these figures to a field gradient determination, the distance between the sensors must be specified. At the present time a spacing of the order of one foot or slightly more is anticipated, therefore, the $\overline{\Delta H}_{min} = 10^{-9}$ gauss corresponds to a gradient measuring capability of at least 10^{-9} gauss/ft or 0.1 mγ/ft.

An advantage of the chart presentation is that the change in performance capability in terms of other values of experimental parameters is readily seen. The signal-to-noise ratios and

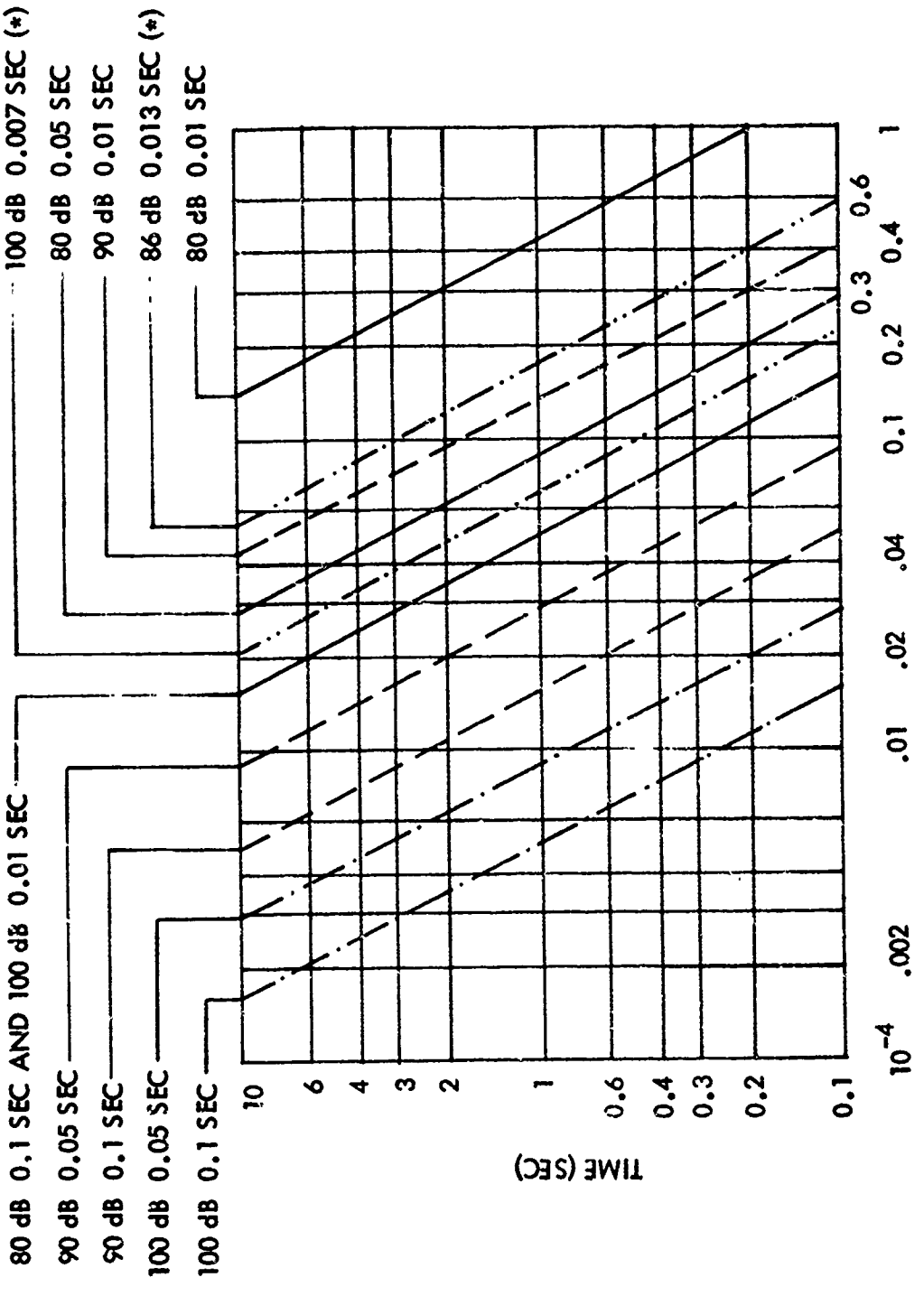

THEORETICAL MAGNETOMETER PERFORMANCE FOR ASSUMED S/N AND T_2.
PREDICTED PERFORMANCE BASED ON EXPERIMENTALLY OBSERVED S/N AND
T_2 FOR BUFFERED AND VACUUM CELLS ALSO INDICATED BY (*).
FIGURE 2-2

39-71-2

relaxation times determined in the experimental program should provide operation of a gradient device in the less-than-10^{-9}-gauss range for required observation times less than 2 seconds.

2.2 PHASE SHIFTS IN THE SPIN GENERATOR LOOP

The spin generator always operates at that frequency for which the net phase shift in the positive feedback loop is zero. If the phase shift is zero in the part of the loop external to the resonance cell itself, the spin generator operates at the center of the resonance line. However, if an external phase shift ϕ is introduced, the spin generator frequency shifts within the resonance line until an equal and opposite internal phase shift is produced. The resulting angular frequency shift $\Delta\omega_\phi$ is given from the steady state solution of Bloch's equations (Ref. 8) as

$$\Delta\omega_\phi = (\tan\phi)/\tau_2, \tag{2-10}$$

where τ_2 is the transverse relaxation time of the magnetic resonance.

In the gradient magnetometer the corresponding error ΔH_ϕ in differential magnetic field measurement will be

$$\Delta H_\phi \sim \delta\phi/(\tau_2\gamma), \tag{2-11}$$

where γ is the gyromagnetic ratio and $\delta\phi$ is the residual difference in external phase shifts in the two spin generator loops.

Let us assume, as will be shown in Section 5 to be reasonable, that a value for τ_2 of 0.01 sec can be achieved at the light intensity levels required to obtain a suitable signal-to-noise ratio. Then, using $\gamma \sim 2.2 \times 10^6$ rad/sec-G, for Cs^{133}, and

$\Delta H \sim 10^{-9}$G, equation (2-11) gives the allowable residual phase shift difference during the integration time as

$$\delta\phi \sim 2.2 \times 10^{-5} \text{ rad.}$$

The electrical phase shift in each spin generator feed-back path can be minimized by using the pick-up coils and the negative feed-back amplifiers with high open-loop gain. The essentially geometrical phase shifts caused by variations in the angle between the readout beam and the direction of the earth's magnetic field become very small when the readout beam is parallel to the direction of H_1, the driving rf magnetic field. An analysis of the geometrical phase shift as a function of the relative orientation of the readout beam and the applied dc magnetic field is given in Reference 6. It is shown that, for perfect parallelism between the readout beam and the H_1 magnetic field, this geometrical phase shift is independent of the direction of the applied dc magnetic field.

2.3 OTHER PERTURBATIONS

The potential sources of error in the gradient magnetometer included in this group are primarily those associated with intrinsic properties of magnetic resonance in the alkali vapors. They include the light-induced frequency shifts, orientation dependence, and rf amplitude dependent shifts.

The light-induced frequency shifts are due to the on-resonance and off-resonance components of the light beams. They are functions of the spectral distribution of the light, intensity of the light, and polarization of the light. Another recently found characteristic is one that involves the presence of the rf field.

The orientation dependence and rf amplitude dependence involve the changes in the population distribution of the various levels involved in the resonance.

In a single sensor, conventional magnetometer, these effects contribute to the relative error and absolute error by their full magnitude. In the gradient magnetometer it is the difference in perturbation on the frequencies of the two spin generators that causes the error. The design of the gradient magnetometer shown schematically in Figure 2-1 is such that these errors will tend to be the same in the two spin generators and thus their effects will tend to balance and cancel out. It is for this reason that both pumping beams are shown to originate from a common beam by means of a beam-splitting polarizer. Changes in intensity and spectral distribution will therefore be common to both cells. The same is true of the light for the two readout beams.

The orientation-dependent shifts will also be common in both cells and will therefore also tend to cancel each other at the output.

The expected differential sensitivity of 10^{-9} G is in a region at the state of the art for cesium. With this sensitivity, additional sources of frequency perturbations may be encountered. Such sources might be temperature or the chemical nature of the wall. Again since the units are being operated in a differential mode, the opportunity exists to minimize these, if they arise, through balancing the characteristics of the two cells.

It should be emphasized that the gradient instrumentation, or two cell approach, permits the utilization of the higher sensitivity now available. Changes in the ambient magnetic field would limit the usefulness of this higher sensitivity if only a single cell were used.

SECTION III

3.0 EXPERIMENTAL WORK

The objectives of the experimental work included fabrication of the resonance cells and establishment of the test conditions to evaluate the cell performance parameters. The equipment was also designed so that it could be operated as a single unit magnetometer under conditions effectively approaching those expected of the dual cell configuration. The essential and special features of the circuitry are also described in this section.

3.1 DESIGN AND TEST OF MAGNETICALLY SHIELDED COIL ASSEMBLY

The physical requirements for the optical pumping apparatus include a uniform dc magnetic field H_o with a pumping beam along its direction and an oscillating rf field polarized perpendicular to H_o with a readout, or cross beam, also perpendicular to H_o. These requirements are to be satisfied at the location of the resonance cell.

The general arrangement of the optical and magnetic field components is shown schematically in Figure 3-1.

The magnetic fields are generated by currents in air-core coils arranged to produce homogeneous fields. A three-layer magnetic shield made of the alloy High-mu 80 surrounds the large coil structure that generates the homogeneous dc magnetic field. The mean diameter of these coils is 17 inches.

The optimum coil spacing and expected variation in the magnitude of the magnetic field were calculated under the assumption that the magnetic material from which the shields were made had infinite permeability. This assumption allowed the use of images

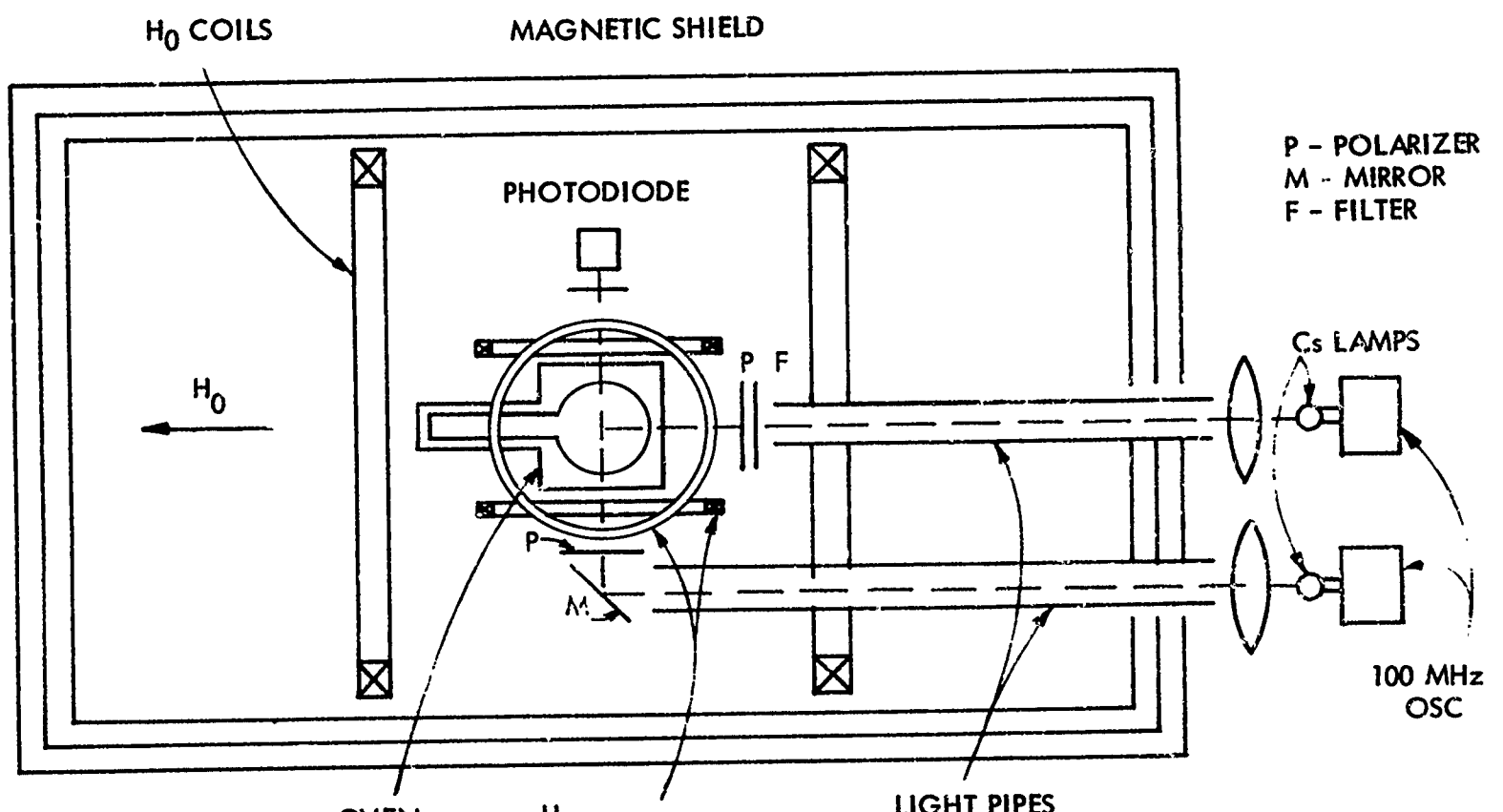

SCHEMATIC DRAWING OF ARRANGEMENT OF APPARATUS ASSOCIATED WITH MAGNETICALLY SHIELDED TESTS.
FIGURE 3-1

to describe the effects of the end plates of the shields on the magnetic field magnitude and homogeneity. The coil separation was adjusted to the calculated value.

The magnitude of the magnetic field was measured along the axis and off the axis of the shielded coil assembly. A compact optically-pumped mercury magnetometer with an accuracy of about 0.01% was used in these measurements. Some improvement in homogeneity was obtained by small empirical adjustments of the coil spacing. The coil spacing and position inside the magnetic shields were then rigidly fixed by means of spacers between the coil forms and the inner surfaces of the shield. The constant magnetic field has a measured variation of about 0.03% over the volume of a cell.

In a field of about 0.1 gauss at which most of the measurements were made, this percentage variation, 0.03%, corresponds to a total field change of 3×10^{-5} gauss. With the theory developed by Cagnac (Ref. 9) for relaxation due to diffusion in a vacuum cell in an inhomogeneous magnetic field, the relaxation time associated with the gradient can be shown to be greater than one second. This makes the effect of inhomogeneity small compared to the values intrinsic to the cell itself.

The oscillating rf magnetic field is provided by two orthogonal pairs of coils about 4 inches in diameter. Circularly polarized rf fields can be produced of either sense of rotation by driving the coil pairs with two signals in quadrature.

The cesium lamps are electrodeless discharge lamps driven by a few watts of 100 MHz rf. Their design and construction are similar to that reported in Ref. 10. Since some of the materials used in constructing the lamps are magnetic, the lamp-oscillator assemblies for some of the tests were located outside the magnetic

shield. The light for the pumping and readout beams was brought into the vicinity of the sample cell through holes in the magnetic shield cans by means of light pipes. Several methods for constructing light pipes were tested. Coating the inside of a glass tube with silver was effective. However, the use of gold-coated Mylar was found to be more efficient and very easy to use as a liner in any convenient tube.

In all of the work with cesium, interference filters were used to isolate the D-1 wavelength 894.3 nm.

The pumping beam is circularly polarized by means of commercial sheet polarizers designed for use at these wavelengths.

The polarization of the cross beam was either circular or linear, depending on the particular experiment being performed. Provisions were also made for having an analyzer in the cross beam.

The cross beam intensity was determined by the photodiode - a custom-made, non-magnetic MOS phototiode.

The resonance cell was contained in a two-zone oven with Pyrex windows to accommodate the light beams. The two zones allowed the independent control of the temperature of the tail and the head of the cells. The ovens were heated by means of a hot air flow. The heaters, of course, were located outside the magnetic shield.

3.2 ELECTRONIC CIRCUITRY

Three general types of magnetic resonance signals were used in evaluating the performance of cesium cells and in the test of components as a single unit optically pumped self-oscillating magnetic resonance magnetometer. The relaxation times of the

resonances were determined by rf pulsed techniques and with shuttered and/or attenuated light beams. Signal-to-noise ratios are first determined using open-loop steady state methods. In the magnetometer experiments the magnetic resonance is observed as the output of an oscillator operating with the cesium cell as the frequency-determining element. Electronic components have been assembled to provide appropriate voltages to drive the coils and to detect and amplify the desired magnetic resonance signals. The current for the dc magnetic field is obtained from a well-regulated, constant-current source.

The pulsed rf circuitry is designed to generate a single pulse or pair of pulses of variable separation, variable amplitude, and independent pulse width. The repetition rate of the single pulse or pair of pulses is also independently variable and can also be made "single shot" with an external trigger. The circuit requirements will be recognized as those generally associated with spin-echo NMR techniques.

A block diagram indicating the major components is shown in Figure 3-2. In order that the resonance signals be uniformly generated, it is desirable that the rf pulses be coherent, i.e. part of the same wave train, and that each pulse begin with the same phase. Each sequence of pulses is initiated by the triggering circuit which either runs repetitively or is itself triggered by an internal pulse from a switch connected to a shutter.

The pulse width and position determining circuit is triggered by a short pulse synchronous with the rf oscillator. The rectangular pulses activate the rf gate which allows portions of the cw signal from the oscillator to pass. The isolation between pulse-on and pulse-off is better than 120 dB

The coherent pulses are applied to the pair of orthogonal coils through the driver amplifiers with one coil being supplied with

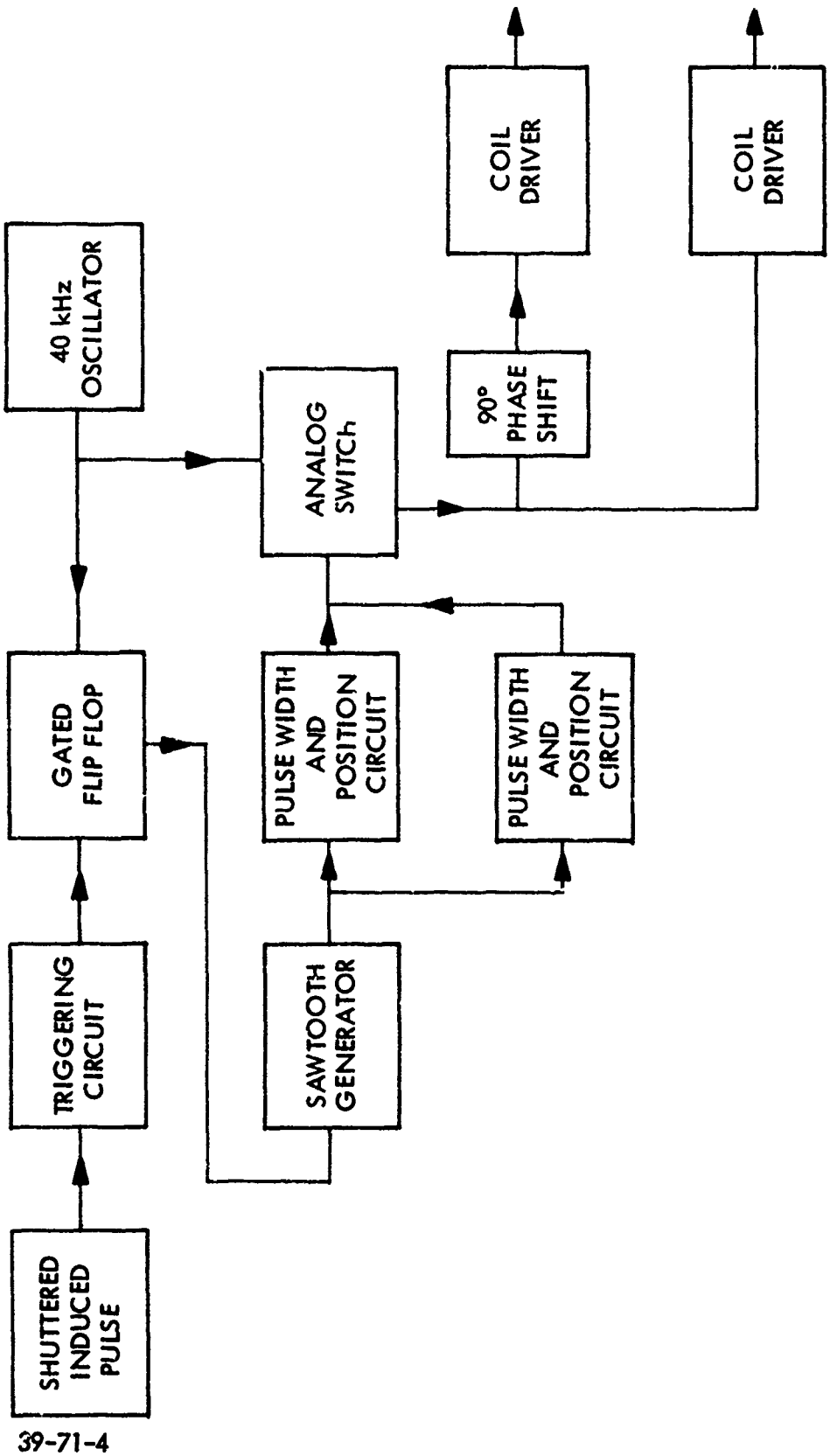

PULSE CIRCUITS FOR RELAXATION TIME MEASUREMENT
FIGURE 3-2

a signal phase-shifted with respect to the other by 90°. The sense of rotation of the rf can be changed by means of a reversing switch between the coil driver circuit and the coil. When steady-state magnetic resonance signals are desired, the input from the pulse width and positioning circuits is disconnected and a suitable dc bias applied. The level of the rf voltage can be adjusted to the desired low level by controls at the oscillator and the gain of the gate circuit.

The magnetic resonance signals are present as amplitude modulation of cross beam light. The light with wavelength 894.3 nm is in the near infrared. The percentage modulation of the beam is a few percent. The intensity of the light is detected by means of a MOS photodiode. Through special arrangements with the manufacturer, a non-magnetic device was obtained. The usual commercial device is in a TO-5 can which is magnetic, as are the Kovar leads.

A circuit for amplifying the signal from the photodiode was designed to minimize the noise due to the circuit elements. The objective was to keep the noise level due to components at, or possibly below, that associated with photocurrent of the diode. The circuit is similar to those usually used. The photocurrent is amplified first by a low noise preamp stage to a level that can be further amplified by an OP AMP with little additional contribution to the noise.

A review of the design principles identified the major sources of noise as the bias current, the shot noise, device noise from the photodiode, load resistor, FET device noise, and OP AMP device noise. Each source was described in terms of experimental parameters and its contribution calculated. A circuit was assembled and noise measured at the output. About half the noise was found to originate in the light beam. This was in

general agreement with the theory. The major problem in computing the noise levels is the variability of the semiconductor devices. For example, the noise from the FET preamp was found significantly below that estimated from the typical characteristics published by the manufacturer. The circuit is shown in Figure 3-3.

3.3 CELL FABRICATION

The cesium cells produced at Singer are classified either as buffered or vacuum cells. The buffered cells contain a buffer gas to reduce the rate of collisions between the cesium atoms and the glass walls. The vacuum cells contain no buffer gas, but have a coating on the interior surfaces. This coating is designed to minimize the interaction between a cesium atom and the wall during a collision.

The buffered cells are produced by the following procedure. A 100 milliliter pyrex sphere is attached to the vacuum system by means of a 7 millimeter O.D. pyrex tube. The diagram in Figure 3-4 shows the pertinent components of the vacuum system.

The portion of the system shown inside the oven is heated to 300°C under vacuum for several hours to drive off gas contained on and in the glass walls. After the system has cooled, the system pressure is typically 10^{-7} Torr. The fragile-tipped ampoule is then opened by means of the glass-enclosed magnet, and the cesium is gently driven into the sphere with a hand-torch. Stopcock A is then closed and the buffer gas is admitted into the cell through stopcock B. The final buffer gas pressure is typically 20 Torr. The cell is then removed from the vacuum system by means of a hand torch at the indicated seal-off point.

A literature search indicated that the best buffer gases were

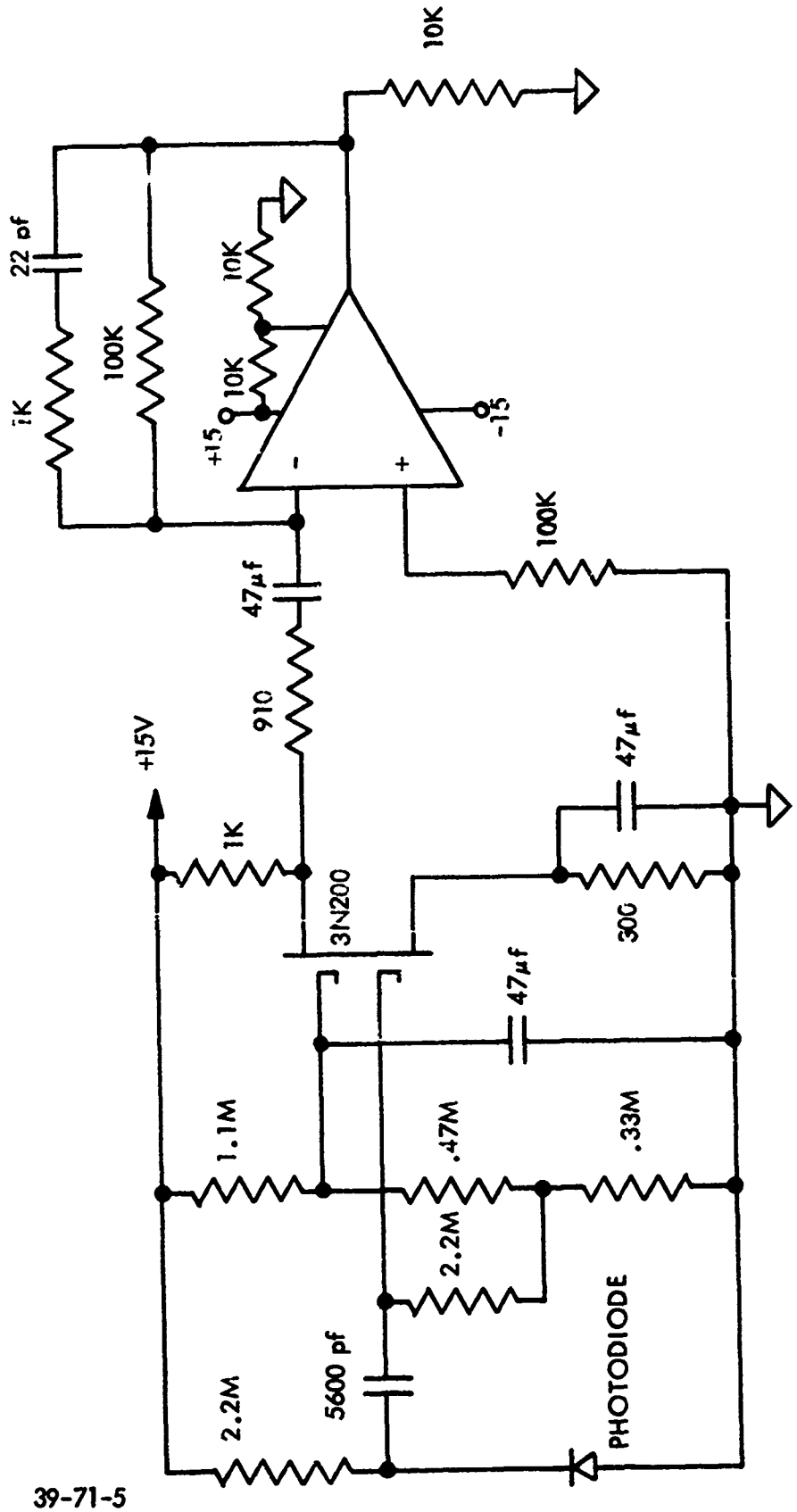

PHOTODIODE AND AMPLIFIER CIRCUIT

FIGURE 3-3

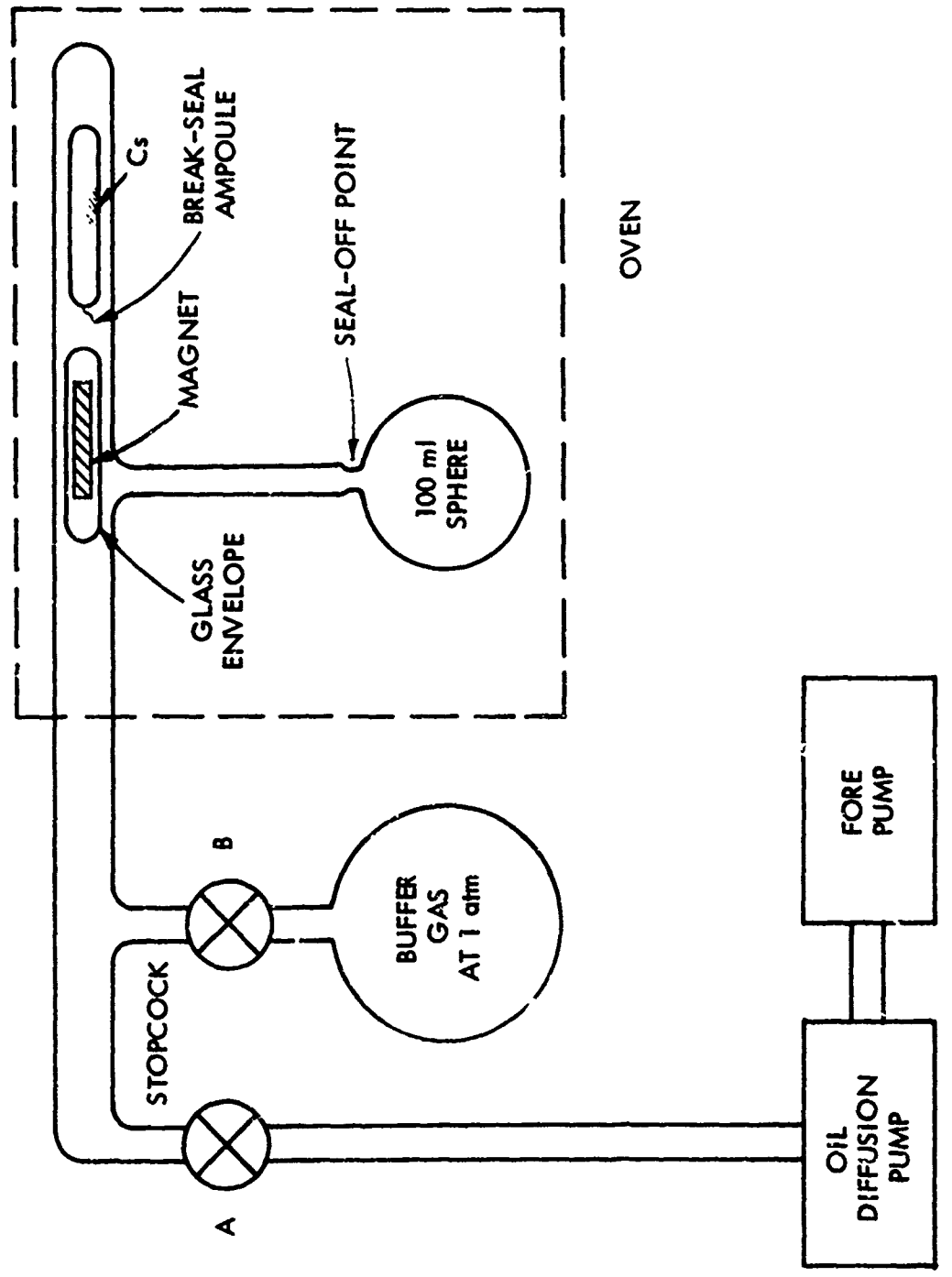

39-71-6

SCHEMATIC DRAWING OF VACUUM SYSTEM FOR FILLING BUFFERED CELLS
FIGURE 3-4

nitrogen and helium. (Refs. 11, 12) Nitrogen was tried first. The longitudinal relaxation time, T_1, and the transverse relaxation time, T_2, were measured in the test apparatus which is described later. The cell with 100 Torr of N_2 had a T_1 of about 200 milliseconds and a T_2 of about 3 milliseconds. The cell with 100 Torr of helium had a T_1 of about 100 milliseconds and a T_2 of about 3 milliseconds.

The more difficult art of producing a vacuum cell was then undertaken. The early work on vacuum cells usually involved Rb rather than Cs (Ref.13). A highly successful effort with Cs was reported quite recently (Ref.14); T_1's of 250 ms were reported. The vacuum system arrangement for producing one of these cells is shown in Figure (3-5).

The sphere has been previously coated with wax on the interior. Many variations were tried in this part of the procedure and will be described below. The cell is heated to about 125°C for several hours under vacuum. After cooling, the system pressure is typically 10^{-6} Torr. The constriction is gently flamed to drive off impurities and the cell is then sealed off from the vacuum system at that point. The two ampoules are then broken by shaking the cell. The purpose of the barium is to getter any gases that might evolve in the sealed-off cell.

The production of a suitable wall coating is the key to a vacuum cell with desirable characteristics. These characteristics include high signal-to-noise ratio, long relaxation times, and long-term performance stability. In order for a cell to have these characteristics, the wall coating must cover the entire interior surface fairly uniformly, transmit infrared light well, interact only weakly with the cesium atoms, and be stable under the cell operating conditions. Several coatings of long-chain hydrocarbons were tried. They include: paraflint, a mixture of

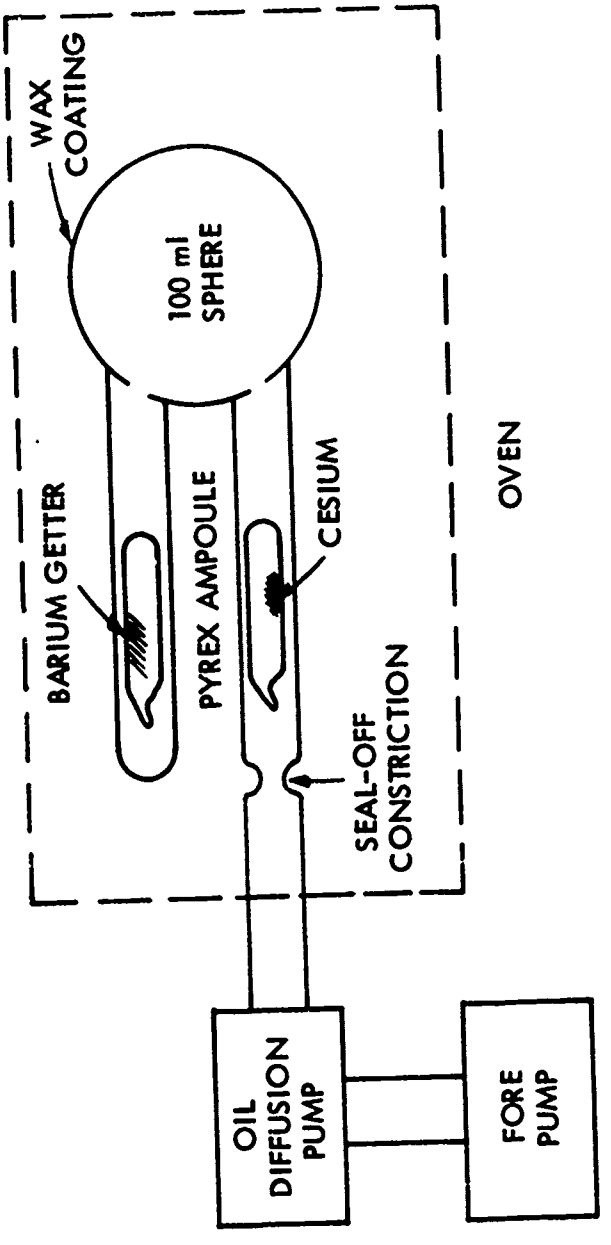

SCHEMATIC DRAWING OF VACUUM SYSTEM FOR PROCESSING WALL-COATED VACUUM CELLS
FIGURE 3-5

39-71-7

saturated hydrocarbons with an average chain length of 50; high-purity hexatriacontane, $C_{36}H_{74}$; high-purity octacosane, $C_{28}H_{58}$; and a mixture of the hexatriacontane and octacosane. These waxes were deposited on the cell wall by a variety of techniques. These include: (1) dissolving a small quantity of wax in a solvent inside the cell, sloshing the solvent around by shaking the cell, and evaporating the solvent out under vacuum; (2) placing a large amount of wax inside the cell, melting the wax, and sloshing the wax around by shaking the cell; (3) baking the cell out under vacuum while keeping the wax in a cool side-arm, melting the wax and running it into the cell under vacuum, sealing the side-arm off from the cell, sealing the cell off from the vacuum system, and sloshing the wax around as in step (2); and (4) baking the cell under vacuum, opening the cell to air, putting the wax in the cell, evacuating the cell, introducing an inert gas at a pressure of a few Torr. and heating the wax gently to evaporate it. The pure waxes individually did not form good wall coatings because they appeared to form large crystals which did not adhere well to the glass wall. The paraflint and a 1-to-1 mixture of the pure waxes did adhere well to the glass wall and did produce promising results. The method of application did not seem to be an important factor in the ultimate cell performance.

Vacuum cells do not produce resonance signals when first put into the crossbeam test apparatus. Weak signals usually appear after a few days and gradually increase with time. The cells seem to "age". The cells are also heated in a controlled fashion during this time to temperatures up to 50°C. The relaxation times of cells that have strongly adhering coatings gradually increase to about 10 milliseconds, with T_1 slightly greater than T_2. If the cells continue to be heated, their performance degrades - the relaxation times decrease. The wax coating can then be melted and the process of gradual signal growth, starting from zero

signal, is repeated. More details of the results of these measurements are to be found in Section 5 of this report.

Some of the steps in the fabrication of the resonance cells were developed as part of a separate project. Some of the cells incorporated in the test program had been fabricated prior to the start of this investigation. For a sense of completeness a description of these techniques has been included in fabrication processes presented above in order to provide a better evaluation of the fabrication methods.

SECTION IV

4.0 ANALYSIS OF THE ZEEMAN RF RESONANCES IN THE ALKALI ATOMS

The first optical pumping resonance experiments were performed in the ground state of sodium atoms in an atomic beam in 1952. In later work optical pumping techniques were extended to the other alkali metals as contained in buffered cells and wall-coated cells. A general review of the field of optical pumping is given by Happer (Ref. 8) and recent work on its application to magnetometers is given in references 1 and 2. The major features of these resonances as they apply to magnetometry will be reviewed in this section. This includes a more precise description of the resonance frequency and its perturbation.

4.1 RESONANCE FREQUENCY

The usual macroscopic picture of magnetic resonance is that of a magnetic dipole moment with angular momentum precessing in a magnetic field. The damping of the precessional motion is balanced by the rf magnetic field rotating at, or near, the precessional frequency, also called the Larmor frequency. This macroscopic picture can be justified in terms of what is happening on the atomic scale by relating the macroscopic moment to the expectation values of the various components of the magnetic moments of the microscopic particles and then summing over all the particles in the sample. This picture and approach are valid for describing the general behavior of most magnetic resonance experiments and is quite exact for those situations with spins of 1/2 or those with no hyperfine structure in the ground state. The dynamics of the net magnetic moment $\vec{M}$ are well described by the phenomenological, modified Bloch equations (Ref. 15):

$$\frac{dM_x}{dt} + \gamma(\vec{M}x\vec{H})_x + \frac{M_x}{\tau_2} = 0$$

$$\frac{dM_y}{dt} + \gamma(\vec{M}x\vec{H})_y + \frac{M_y}{\tau_2} = 0 \qquad (4\text{-}1)$$

$$\frac{dM_z}{dt} + \gamma(\vec{M}x\vec{H})_z + \frac{M_z}{\tau_1} = \frac{M_o}{\tau_1} \quad .$$

The relaxation times τ_1 and τ_2, the longitudinal and transverse relaxation times, each have three contributions, the intrinsic relaxation time of the atoms in the cell, the relaxation caused by the pumping beam, and the relaxation caused by the readout beam. This can be expressed as

$$\tau_1^{-1} = T_1^{-1} + aT_{px}^{-1} + bT_{pz}^{-1}$$

$$\tau_2^{-1} = T_2^{-1} + T_{px}^{-1} + T_{pz}^{-1} \qquad (4\text{-}2)$$

Where T_1 and T_2 are the intrinsic or thermal relaxation times and T_{px} and T_{pz} are the mean times between absorption by an atom of consecutive photons from the crossbeam and from the readout beam. T_{px}^{-1} and T_{pz}^{-1} are proportional to the intensity of the respective light beams and a and b are numbers close to unity.

The total field $\vec{H}$ is assumed to have a dc component H_o along the z direction and an oscillating part perpendicular to H_o. The resonance frequency is $\omega_o = \gamma H_o$ where γ is the gyromagnetic ratio.

A spin of 1/2 in a magnetic field has two time independent stationary states of + 1/2 and - 1/2, as sketched in Figure 4-1.

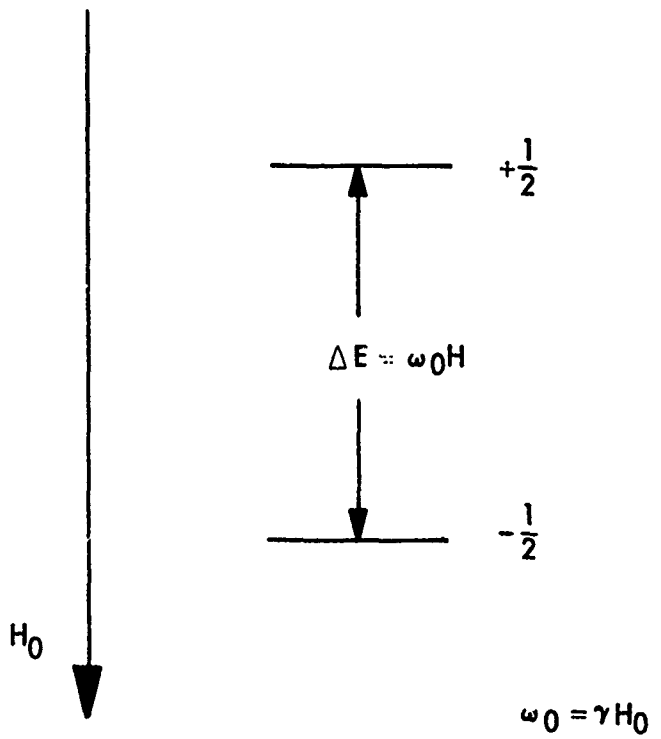

39-71-7

ENERGY LEVEL DIAGRAM FOR
ZEEMAN LEVELS OF SPIN 1/2
FIGURE 4-1

The energy separation between the states is $\Delta E = \omega_o h$, where ω_o is the Larmor frequency and h is Planck's constant divided by 2π. The orientation resulting in the net magnetic moment M_o in equation 4-1 is due to an unequal population in the two levels. The precessing magnetic moment is described in this picture as a coherence between these two levels, or alternatively, that the atom is in a time dependent superposition of these two levels.

In the case of the ground state of the alkali metal atoms, the total angular momentum F is the sum of the nuclear magnetic momentum I and the electron angular momentum J = 1/2. For cesium I = 7/2, therefore there are two ground state hyperfine levels F = 3 and F = 4. The separation between these levels is 9.19 GHz. In a magnetic field each F-level splits into the 2F+1 Zeeman level m_F = 4,3,..., -3, -4, and m_F = 3,2,..., -2, -3.

The magnetic resonance occurs between adjacent m_F-levels. The separation between the various levels are not equal. The energy of each m_F level is given by the Breit-Rabi formula. Therefore basically there are a total of 8 resonance frequencies in the F = 4 level and 6 in the F = 3 level. In low magnetic fields, of the order of 1 gauss that would be encountered in the earth's magnetic field, these frequency differences are not very large compared to the average separation of the Zeeman levels. To a fair approximation the components can be calculated in the following way. The average Larmor frequency is

$$f_o = 2.8 \times 10^6 \, H_o/(2I+1) \qquad (4\text{-}3)$$

which for Cs^{133} is

$$f_o = 3.5 \times 10^5 \, H_o \qquad (4\text{-}4)$$

where H_o is in gauss and f_o is in Hz. The F = 3 group of resonances and F = 4 group of resonances are separated by

$$\Delta f = 2\gamma_n H_o \ , \tag{4-5}$$

where γ_n is the nuclear gyromagnetic ratio divided by 2π. For Cs^{133} this is

$$\Delta f = 1123.4\ H_o \ . \tag{4-6}$$

The separation between each of the components of F = 3 group or of the F = 4 group is

$$\delta f = 2\gamma_o^2 / f_{hfs} \ ,$$

where f_{hfs} is the separation of the hyperfine levels.

Two examples of typical frequencies and separations are shown for Cs^{133} in Table 4-1.

Table 4-1 Resonance Frequency for Cs^{133} in a Magnetic Field of 0.114G and 0.5G

	H_o = .114 G	H_o = 0.5 G
f_o, Average Frequency Separation of Zeeman Components	4×10^4 Hz	1.75×10^5 Hz
Δf, Separation of F = 3 and F = 4 groups	128 Hz	562 Hz
δf, Separation of resonances in F = 3 and F = 4	0.345 Hz	6.7 Hz

The relative amplitudes of the various components of the resonance depend upon the degree of orientation established by the light beams. This is a function of the intensity, degree of polarization, and orientation of the light beam with respect to the magnetic field. Meilleroux (Ref. 16) gives a good discussion of this topic.

As an example of this effect, the Zeeman levels are shown diagramatically in Figure 4-2 for the F = 4 level. To the right of the level diagram the relative populations of the various m_F levels are sketched in. In the drawing below, the relative populations are translated into amplitudes of resonances between adjacent m_F levels. The composite resonance line is sketched in as a dashed curve. The linewidth was chosen to be slightly less than the separation between the various components. It should be emphasized that this line structure represents what would be observed if the frequency were swept while the H_o field remained constant.

To an extent, this group of resonances can be described by considering each component as resulting from a fictitious spin of 1/2 associated with each pair of levels. The validity of this description depends upon how well resolved the individual components are. A more accurate description becomes complicated by the fact that the various resonance components are not independent of each other but are coupled: the lower state of one pair of levels is the upper state of the adjacent resonance. Under such conditions the most convenient description is in terms of the density matrix formulation. Happer shows that if the density matrix is represented in terms of spherical basis operators, the various properties of the resonances can be discussed in terms of various multipole polarizations. The usual Bloch type resonances correspond to the dipole part.

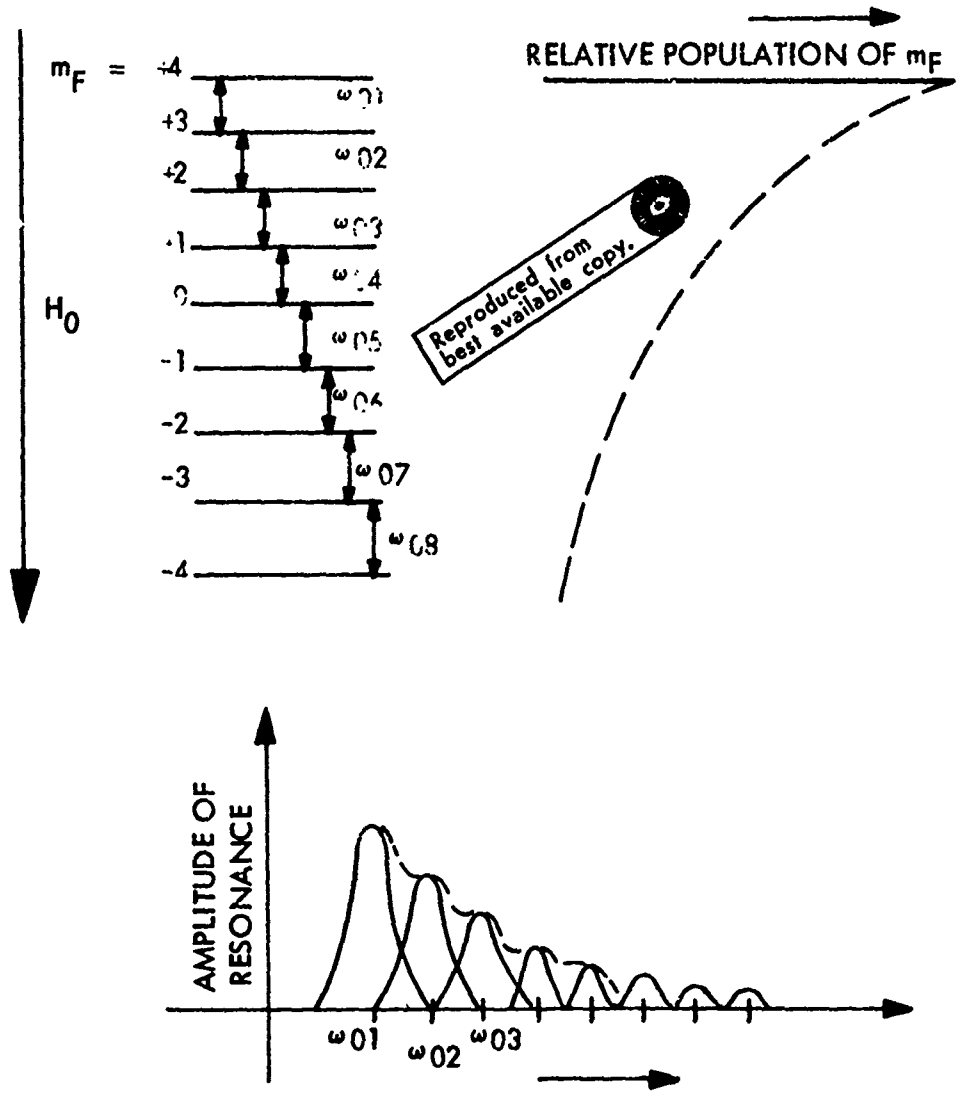

39-71-8

ENERGY LEVEL DIAGRAM OF ZEEMAN LEVELS FOR F=4 HYPERFINE LEVEL AND LINE SHAPE FOR ASSUMED POPULATION DISTRIBUTION

FIGURE 4-2

In the case that the resonances are observed as the output of a spin generator, the frequency of oscillation will be fixed at the value where the phase response for the composite resonance goes through zero, which should be quite close to the peak of the largest resonance. The instrumentation must be designed such that any changes in the frequency of oscillation are due only to changes in the H_o field. In the design of a gradient magnetometer, there are two such self-oscillating units and here the primary requirement is that the difference in frequencies reflect only a difference in field. If a perturbation has the same effect on both oscillators, the difference between the output frequencies will be zero.

4.2 PERTURBATIONS OF THE RESONANCE FREQUENCIES

In this section the various sources of perturbation to the resonance frequency that are associated with the fundamental properties of the cesium itself will be reviewed. The perturbation associated with the geometry of the apparatus was discussed in Section 2.2. The principal sources of frequency shift are associated with the rf drive and with the light beam.

The rf field can affect the resonance frequency in two ways. The most familiar arise when a linearly polarized field is used to drive the resonance. The shift in frequency is due to the counter rotating component of the H_1 field; this is known as the Bloch-Siegert shift (Ref. 17). This shift can be eliminated by using a circularly polarized field, as has been done in the relaxation experiments since a circularly polarized field is used to select the group of resonances in one hyperfine level in preference to those in the other.

Having selected the resonance to take place in say the F = 4 hyperfine level, the amplitude of the rf can cause a shift in

the apparent resonance frequency. As the rf field amplitude increases, the components of the resonance broaden and the relative amplitudes of the components will tend to equalize. This in spin generator operation will tend to shift the zero phase point of the resonance. Without knowledge of the specific light intensities and intrinsic linewidths employed, estimates of the value for this shift would not be meaningful.

Development of a theory for the light induced frequency shifts has begun. Applying to cesium the techniques used for calculating the shifts in mercury, it is found that the computer requirements are quite a bit more extensive compared to those required for handling mercury-201. The calculations involve a numercial solution of the Liouville equation which is a first order differential equation for the rate of change of the density matrix. In the coupled representation this involved many inversions of a 15 x 15 complex matrix for mercury-201, which has a ground state angular momentum F = 3/2. The equivalent formulation for the cesium F = 4 level would be an 80 x 80 complex matrix.

In consultation with Happer an alternate approach was sought. General expressions have been obtained in which the magnetic resonance lineshapes are expressed in a power series of the light intensity. The series is rapidly convergent under normal experimental conditions, and the first two terms in the series are adequate to describe the shift and distortion of the magnetic resonance lineshapes under the influence of the pumping light and the small quadratic splitting of the upper Zeeman multiplet of the alkali atom due to perturbations by the lower multiplet. The magnetic resonance lineshapes themselves can be expressed in terms of certain simple resonance lineshapes, the classical Bloch functions, which are connected with resonances monitored by circularly polarized light, and the less well known Series resonances, which are connected with resonances monitored by linearly polarized

light. Some of the light-induced shifts in these resonances depend on the radio-frequency power, and they can actually reverse sign as the power increases. These power-dependent shifts have nothing in common with the well known Bloch-Siegert type of shift.

From these general expressions, the lineshapes and displacements may be calculated for particular orientations of polarizers and analyzers. The optical spectral distribution may also be included. With the aid of these calculations the magnitude of the light induced frequency shifts may be estimated. The lineshape curves can serve as a guide to identifying them in experiments and in reducing their influence on the performance capabilities of the magnetometer.

SECTION V

5.0 MEASUREMENT OF CELL PARAMETERS

As indicated in Section 2.1, the performance of a gradient magnetometer can be directly related to the signal-to-noise ratio and relaxation times of the resonance cells that are used. The apparatus employed in measuring the longitudinal relaxation time T_1 and transverse relaxation time T_2 is described in Section 3.2. The particular test methods employed and the results of the measurements are described in this section.

5.1 TEST METHODS EMPLOYED

Transient techniques were used to determine relaxation times. These methods are closely related to the Carr-Purcell 90°-180° spin echo techniques (Ref. 18) and provide direct measurement of the relaxation times with the light beams illuminating the cell, that is without the effects of the rf field. With the use of the shutter in the pumping beam and attenuators in the readout beam, the contribution from the light on the observed relaxation rates can be assessed and eliminated from the total rate where necessary.

The procedure for measuring the transverse relaxation time is as follows. The magnetic moment is established along the direction of the dc magnetic field H_o by means of the pumping beam. No rf is on during the pump-up time. A 90° rf pulse causes the net magnetization to nutate through 90°, after which the transverse magnetization precesses about H_o and decays to zero. The amplitude of modulation of the crossbeam is proportional to the magnitude of the magnetization. The modulation is detected by means of the photodetector and amplified. The output of the amplifier can be displayed on an oscilloscope which shows a damped oscillation. The transverse relaxation times of the magnetic resonance can thus be obtained from the scope display.

As discussed in Section 4, the light beams themselves may contribute to the decay. To eliminate this effect, the pumping beam can be shuttered when the 90° pulse is applied; any change in decay time is due to the pumping beam. The effect of the readout beam can be determined by first measuring the decay with the full intensity and following this with a second measurement at about half the original intensity. A linear extrapolation of these two measurements to zero light intensity gives the intrinsic relaxation time T_2.

The longitudinal relaxation time T_1 is measured with a 180°-90° sequence. A 130° pulse inverts the direction of the net magnetic moment from being parallel to H_o to being antiparallel to H_o. If the pumping beam is on, the magnetization if unperturbed decays through zero and on to its equilibrium value parallel to H_o. When a 90° pulse is applied at a time t after the inversion by the 180°, the magnetization existing at that time is rotated up to the transverse plane and its magnitude can be sensed by the crossbeam. If the 90° pulse is applied at the time t_{null} when the magnetization goes through zero, the relaxation time T_1 is just $t_{null}/.693$.

In the case that the pump beam is turned off, no 180° pulse need be applied; the 90° pulse is applied at varying times after the beam is turned off. The envelope of the signal amplitudes after the pulses decays with the time constant T_1. The effects of the readout beam can be found in the same way as described above for T_2 by repeating the same set of measurements at two different crossbeam intensities.

The signal-to-noise ratios are determined in a conventional cw or steady state experiment. A weak cw rf signal is applied at a level below saturation and the signal amplitude measured on a wave analyzer tuned to the resonance frequency. The noise is obtained by eliminating the signal by detuning the value of the magnetic field. The noise level is therefore determined at the same frequency setting.

An additional experimental parameter proves useful; it is the total intensity of the crossbeam. The intensity of the crossbeam provides an approximate measure of the density of the cesium vapor. The more cesium atoms present the more the beam is attenuated.

In the original configuration of the shielded test assembly, the pumping and readout lamps were inside the shielded assembly. With the lamps close to the sample cell, the light could be efficiently focused by means of simple glass lenses. The intensities of the pump and readout beam are higher under these operating conditions than when the lamps are outside the shielded assembly and the beams brought in by means of light pipes through small holes (about one inch in diameter) in the shield cans. With the present apparatus achievement of both operating conditions, high light intensity and high field homogeneity, was not attempted. The use of larger diameter light pipes would bring the light intensity up, but this would also require putting larger holes through the shield can. Increasing the size of the holes in the magnetic shield has the potential of decreasing the homogeneity of the magnetic field at the site of the resonance cell.

The measurements of maximum signal-to-noise and demonstration of magnetometer performance were performed with the lamps inside the shielded assembly. The measurements of relaxation times were performed with the lamps outside. Signal-to-noise ratios were also measured at the same time as the relaxation times but these are less than the maximum values obtained with the lamps inside the shield.

5.2 MEASUREMENT OF SIGNAL-TO-NOISE RATIO

Signal-to-noise ratios were measured with the apparatus operating as a spin-generator, i.e. a self-oscillating magnetometer arrangement. In this configuration, the output of the rf amplifier is

connected to H_1 drive coils. The lamps as described in Section 5.1 were inside the shielded assembly.

The cell employed in these measurements was a spherical cell, 6.3 cm in diameter, containing cesium and a buffer gas of nitrogen at about 20 Torr. Both light beams were circularly polarized and both beams filtered to pass only the D_1 component at 894.3 nm.

The signal amplitude at the output of the rf amplifier was measured by means of a wave analyzer tuned to the resonance frequency which was 44 kHz. The signal amplitude was 400 mv (rms). The noise level at this frequency was measured as 10 μv (rms) in the 7 Hz bandwidth of the wave analyzer. The ratio of signal power to noise power per Hz calculated from these measurements is 100 dB. This value of signal-to-noise ratio was observed repeatedly. These conditions of operation and high signal-to-noise ratio were employed during the magnetometer tests described below in Section 6.0.

5.3 MEASUREMENTS OF RELAXATION TIMES

The transverse and longitudinal relaxation times were measured for more than twenty different cells. Some of the cells were filled with a buffer gas, but most of the cells were of the vacuum, wall-coated type. The techniques for fabricating the cells are described in Section 3.3 and the equipment with which the measurements were made is described in Section 3.2. In some cases, signal-to-noise ratio and transmitted light intensity were also measured under the same conditions as the relaxation time measurement.

5.3.1 Buffered Cells

The cell used in the maximum signal-to-noise ratio measurements is a cell buffered with 20 Torr of nitrogen. This cell was selected as typical of the nitrogen buffered cells and detailed measurements made of its parameters. The experimental parameters of this cell were also studied as a function of the temperature of the cell in an effort to determine why the cell behaves as it does and to see if the performance could be improved by working with it at a different temperature.

Two cesium cells were filled with helium as the buffer gas. In one cell the pressure was adjusted to 90 Torr and in the second cell it was adjusted to 200 Torr. The measurements on these two cells are compared. From the literature on optical pumping it was found that the longitudinal relaxation time appeared to be long in cells with helium buffer gases. However, there is little published information on the transverse relaxation times under similar conditions. The measurements reported here were an effort to determine these two parameters under the same experimental conditions. Both parameters are necessary for evaluation of the usefulness of this combination for application to the magnetometer.

Typical of the results of the measurements on the cells with nitrogen buffer gases are the data shown in Figure 5-1. In this experiment τ_1, τ_2, T_1, signal-to-noise ratio, and transmitted light intensity were measured at eight temperatures between room temperature and 58°C. Under these experimental conditions the transverse relaxation time T_2 did not differ greatly from the observed τ_2, that is the light did not affect the value of the transverse relaxation time very much. Therefore only one quantity is shown. The values of T_1, on the other hand being considerably longer, are more strongly affected by the light. To demonstrate this at the higher temperatures where T_1 is longer,

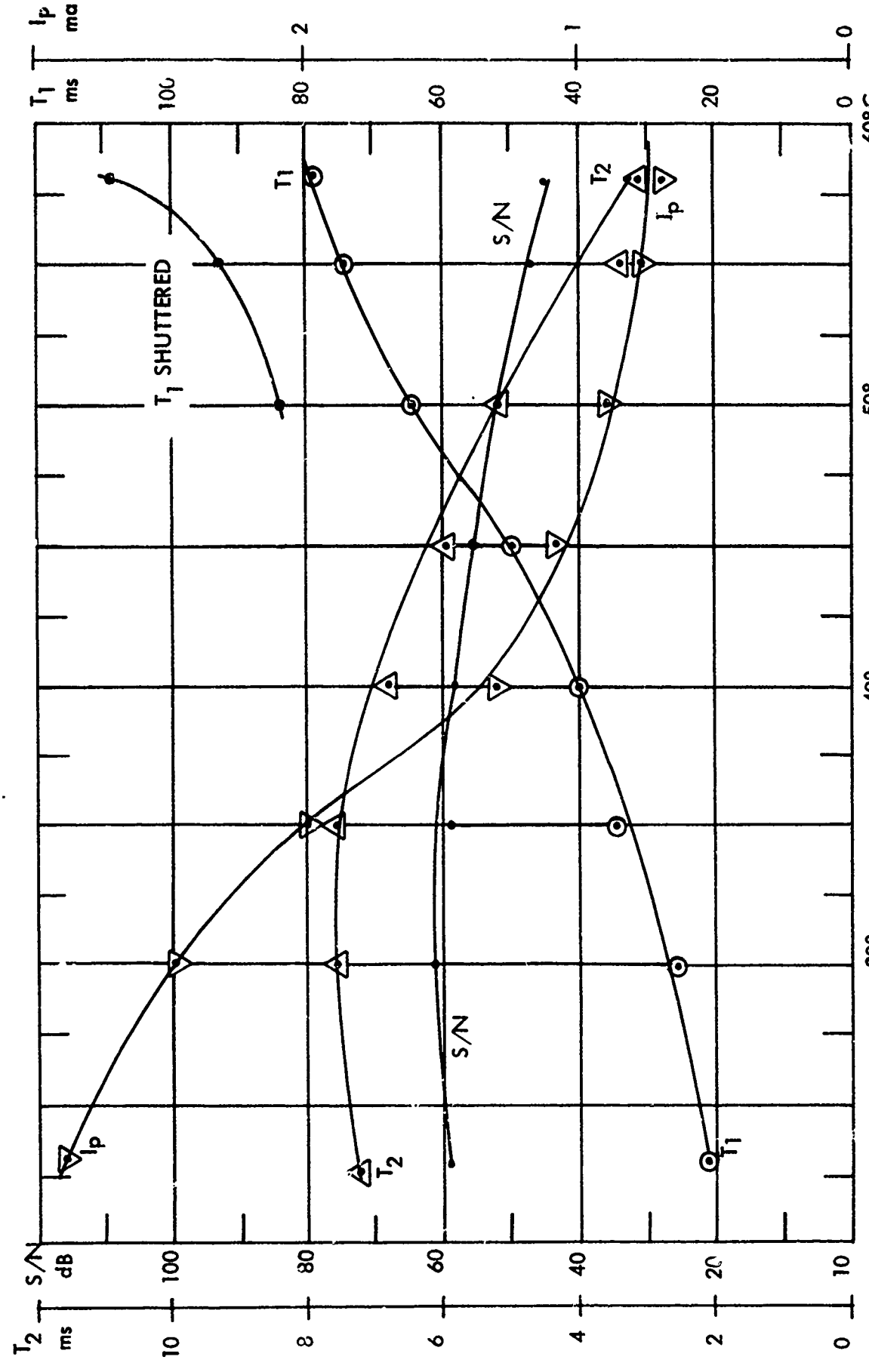

39-71-9

T_1, T_2, SIGNAL-TO-NOISE RATIO IN 7 Hz BANDWIDTH, AND AVERAGE PHOTOCURRENT FOR N_2 - BUFFERED CESIUM CELL AS FUNCTIONS OF TEMPERATURE

FIGURE 5-1

the longitudinal relaxation times were measured with the pump beam shuttered. The observed values are then a combination of the intrinsic relaxation time T_1 and the damping due to the readout beam. The signal-to-noise ratio did not change very much over this temperature range, while the transverse relaxation time decreased after a very small rise near 35°C. The decrease of the photocurrent, proportional to the average intensity of the transmitted crossbeam is due to the increase in density of atoms with rising temperature.

It can be concluded from these data that little is to be gained in magnetometer performance by operating at above room temperature with this type of cell.

The signal-to-noise ratios observed with the lamps outside the shielded test assembly were quite sensitive to the motion of the light pipes. When carefully aligned, the maximum value obtained was about 80 dB (one Hz) with the nitrogen-buffered cell. As indicated previously this loss of 20 dB from the 100 dB obtained with the lights in the can is due to the lower light intensity.

Two cesium cells were filled with helium as the buffer. The helium is spectroscopic grade. The pressure of the helium in one cell was adjusted to 90 Torr and in the second cell to 200 Torr. The relaxation times were measured at several light intensities and extrapolated to zero light intensity to obtain the intrinsic relaxation times. The results are shown in Table 5-1, where the transverse and longitudinal relaxation times for the two cells are listed for the full light intensity and zero light intensity.

Table 5-1 Longitudinal and Transverse Relaxation Times for Helium Buffer Cesium Cells

	He at 90 Torr		He at 200 Torr	
	T_1	T_2	T_1	T_2
Full light intensity	58 ms	3 ms	83 ms	∿3 ms
Zero light intensity	230 ms	3 ms	330 ms	3 ms

The intrinsic longitudinal relaxation times in helium buffered cells are considerably longer than with nitrogen. The observed relaxation times are shortened by the light.

5.3.2 Measurement of Relaxation Times in Vacuum, Wall-coated Cells

The vacuum wall-coated cells, that were tested, were prepared in several ways in that different materials were used to coat the walls and the means for applying the coatings were varied. Several arrangements of cell geometry were tried in which position of the side arms containing the cesium and the getter were varied. The best results in terms of obtaining a strong signal were obtained with the cesium introduced as a sealed-off ampoule in one side arm and the barium getter introduced in a second sealed-off ampoule in a second side arm as described in Section 3.3.

The cells that worked exhibited the following general behavior. Immediately after seal-off from the vacuum system, no signals are observed. Allowing the cells to remain at room temperature for several days usually results in extremely weak signals (a few dB above noise) and very short relaxation times (a few tenths of a

millisecond). If the cell temperature is raised to 30° to 40°C, the signal is observed to grow over a period of hours. The relaxation times are also observed to increase during this heating. A maximum is reached within several hours. If allowed to cool overnight, the cell performance the next day at room temperature is much improved compared to that previously observed at room temperature and not very much different from that observed at high temperature on the preceding day. With several cycles of heating and cooling over a period of days the cells reach an acceptable level of performance.

The performance of cell C-9 can be taken as typical. The wall coating on C-9 is paraflint and in this cell the coating was applied to a vacuum baked out surface by running the paraflint into the cell from a side-arm under vacuum. The wax was melted in an oil bath of about 110°C and run around the walls. The side arm was removed and the cell opened to air and sealed back on the vacuum system with the getter and cesium ampoules in their side arms. The cell was baked at 125° and then sealed off from the system after which the ampoules were broken.

The day after the cell was removed from the system a signal at a level of 85 μv and noise 10 μv was observed. Three days later the level was 115 μv and remained at that level for about a week. After about two weeks of heat cycling, the signal level was 5.9 mv with the cell at 40°C, τ_1 = 13 msec, τ_2 = 11.1 msec, S/N = 63 dB per Hz. These measurements were repeated the following day with the cell at room temperature.

The paraflint was melted at this point and no signals initially observed. After three hours at room temperature the signals became larger than previously observed with much longer relaxation times. The optics were realigned to maximize the signal amplitude, (recall the lamps are outside the shield for these measurements). The signal amplitude was 7.8 mV, τ_1 = 17.4 msec, τ_2 = 12.9 msec, S/N = 66 dB/Hz.

Similar behavior was found for cells coated with a mixture of the pure waxes n-hexatricontane ($C_{36}H_{74}$) and n-octacosane ($C_{28}H_{58}$). Cells coated with a single wax gave much poorer performance. This appears to be due to a non-uniform coating of the glass by the pure wax, which tends to form small crystalline-like regions.

5.4 DISCUSSION OF RESULTS

The potential performance of a gradient magnetometer constructed with cesium cells having the experimentally observed signal-to-noise ratio and relaxation times can be estimated in terms of the analysis as displayed in Figure 1-1. The information present in this figure shows the functional dependence for the detection of a minimum value of change in magnetic field on the time of observation, for a family of values for the experimental parameters: signal-to-noise ratio and relaxation time. The two contributing sources of error are assumed for this calculation to be: the limitation in ability to measure phase in the presence of noise, and the growing perturbation of the phase of the magnetic resonance controlled oscillator by its feedback of noise. The objective of this work is to devise techniques for getting down to sensitivities of 0.1 mγ or less, that is 10^{-9} gauss. It is assumed that one or two seconds would be the time for observation. From Figure 1, it is seen that the line defining 90 dB and 10 msec is just within this range. With 80 dB a relaxation time of 50 ms is within the desired region. With a signal-to-noise of 100 dB and a relaxation time of 10 ms, observation times of one or two seconds give sensitivities in the low 10^{-10} range.

The pertinent experimental data on signal-to-noise ratio and relaxation time are summarized in Table 5-2.

Table 5-2 Summary of Signal-to-Noise Ratio and Relaxation Time Measurements

	Lamps Inside the Magnetic Shields	Lamps Outside the Magnetic Shields	
	Signal-to-Noise Ratio (1 Hz)	Signal-to-Noise Ratio (1 Hz)	T_2 (ms)
N_2-Buffered Cell	100 dB	80 dB	7
Vacuum Cell	--	66 dB	12.9

The maximum signal-to-noise ratio is 100 dB. Under different experimental conditions for the same cell the relaxation time was 7 msec and signal-to-noise ratio about 80 dB. The difference between the maximum value 100 dB and this value 80 dB is attributed to the difference in light intensity for both the pumping and readout beams. It is expected that most, if not all, of the lost 20 dB will be recovered when the restriction in beam diameter imposed by the holes in the shield cans are removed. This demonstrates achievement of the experimental conditions required for having a sensitivity of detecting a field change of 0.1 mγ in one or two seconds.

SECTION VI

6.0 MAGNETOMETER TESTS

The magnetic resonance circuit in which the magnetic resonance signal is applied to H_1 coils is similar to the conventional self-oscillating magnetometer. The frequency of oscillation is, as is described in Section 2, ideally proportional to the magnitude of the magnetic field. For these measurements, the magnetic resonance equipment was connected in this arrangement with the pump lamp and readout lamp inside the shield can. The cell used in these experiments was filled with 20 Torr of nitrogen. This is the cell described in Section 5.3.1. All tests were performed at room temperature. The crossbeam was circularly polarized.

6.1 DESCRIPTION OF THE TEST METHODS

The magnetic shield consists of three concentric closed cans with several one inch holes to accommodate the cables and light beams. The shields have in tests been shown to attenuate dc and low frequency magnetic fields by a factor of about 200. The mean value of the ambient magnetic field in the laboratory is about 0.5 gauss and can change unpredictably by several percent. This means that the field inside the shield can easily change by several gamma (10^{-5} gauss). To measure the sensitivity of the single unit magnetometer directly would require sensing the changes in the ambient field in the laboratory and compensating for them. This would add to the experimental complexity. An alternate method can be used and is outlined below.

It is well known (Ref. 19) that the response of a self-oscillating magnetometer to changes in the magnitude of the magnetic field is practically instantaneous. As yet no lag has been detected. Thus

if the dc field is modulated by a magnetic field changing at a fixed frequency, the frequency of oscillation of the spin generator will also be modulated at this fixed frequency. It is well known from the theory of FM modulation that the spectrum consists of a strong central frequency component with side bands spaced about it at frequencies which differ by integral multiples of the modulating frequency. The amplitudes of the various sideband components are proportional to the Bessel functions, $J(x)$, where x is the ratio of the frequency excursion to the frequency of modulation. Thus if H_m is the amplitude of the modulating magnetic field along H_o and it is at frequency ω_m, the output of the magnetometer will consist of a central frequency component at $\omega_o = \gamma H_o$, with amplitude proportional to $J_o(x)$ where $x = \gamma H_m/\omega_m$ and sidebands at frequencies $\omega_o \pm n\omega_m$ with amplitudes proportional to $J_m(x)$. If $x << 1$, then $J_o(x) \approx 1$ and $J_1(x) \approx \frac{x}{2}$.

This property of spin generators permits the introduction of a change in field value at a frequency where the amplitude of the spectrum due to random changes in the ambient magnetic field is low. In practice most of the spectrum of the ambient field is at the low end of the spectrum, under a hundred Hertz. There also exist strong 60 Hz, 120 Hz and 180 Hz components that arise from the AC lines, overhead lamps, and power supplies.

The test of magnetometer sensitivity consisted of modulating the H_o magnetic field with an alternating field of very low amplitude - a few tenths of a microgauss. The frequency of the modulating field is chosen to be outside the region of modulation caused by the ambient field. Typical frequencies are 90 Hz, 150 Hz, and 250 Hz. The amplitude of modulation can be determined from a comparison of the amplitudes of the central component A_o at ω_o and the amplitude of the first sideband A_1 at $\omega_o \pm \omega_m$.

$$H_m = \frac{2\omega_m}{\gamma} \frac{A_1}{A_o} \quad . \tag{6-1}$$

The signal-to-noise ratio is the limiting factor in determining A_1. Its influence is discussed in the Section 6.2 below.

6.2 TEST PROCEDURES

The coil forms with the windings for the H_o coil contain a second set of windings with independent terminals from the main windings. The modulation is introduced by applying an ac signal of the desired frequency and amplitude to the terminals of the auxiliary windings. The magnitude of the modulating field for a given current can be calculated from the geometry of the coils. The calculations also included the effects of the shield cans on the fields produced by assuming infinite permeability and using the method of images. At low frequencies this gives an accuracy of about 10% and is less accurate at higher frequencies.

The auxiliary coils are tightly coupled by mutual inductance with the principal windings of the H_o coils. The current for the H_o windings is usually provided by a well-regulated, constant-current source, which tends to reduce the pickup in the principal windings and thus reduce the amplitude of the field modulation. Therefore, during the tests on magnetometer operation, the current source for the principal windings on the H_o coil was a battery. A large inductance in series with the battery and coils served to block the flow of any currents tending to cancel the modulating fields.

The amplitudes of the frequency components of the output of the magnetometer were determined by means of a wave analyzer with a 7 Hz bandwidth. In some cases the output of the wave analyzer was plotted with an X-Y recorder. A tracing of a portion of a

typical curve is shown in Figure 6-1. The frequency of the modulating signal was 90 Hz. The calculated level of the signal was 0.2 μG. The magnetometer-measured level of the perturbing field is 0.180 ± 0.024 μG. The uncertainty in the measurement is 0.024 μG or 2.4 milligamma in the 7 Hz bandwidth of the wave analyzer. If we assume the uncertainty to vary in the same way as noise with bandwidth, then in a 1 Hz bandwidth, this corresponds to an uncertainty of about 1 milligamma. If the magnetic environment were quieter, the measurements could be performed at a lower frequency where by equation (6-1) it is seen that 0.1 mγ sensitivity would be obtained if the field were applied at about 5 Hz. The experimental results are in reasonable agreement with the theory.

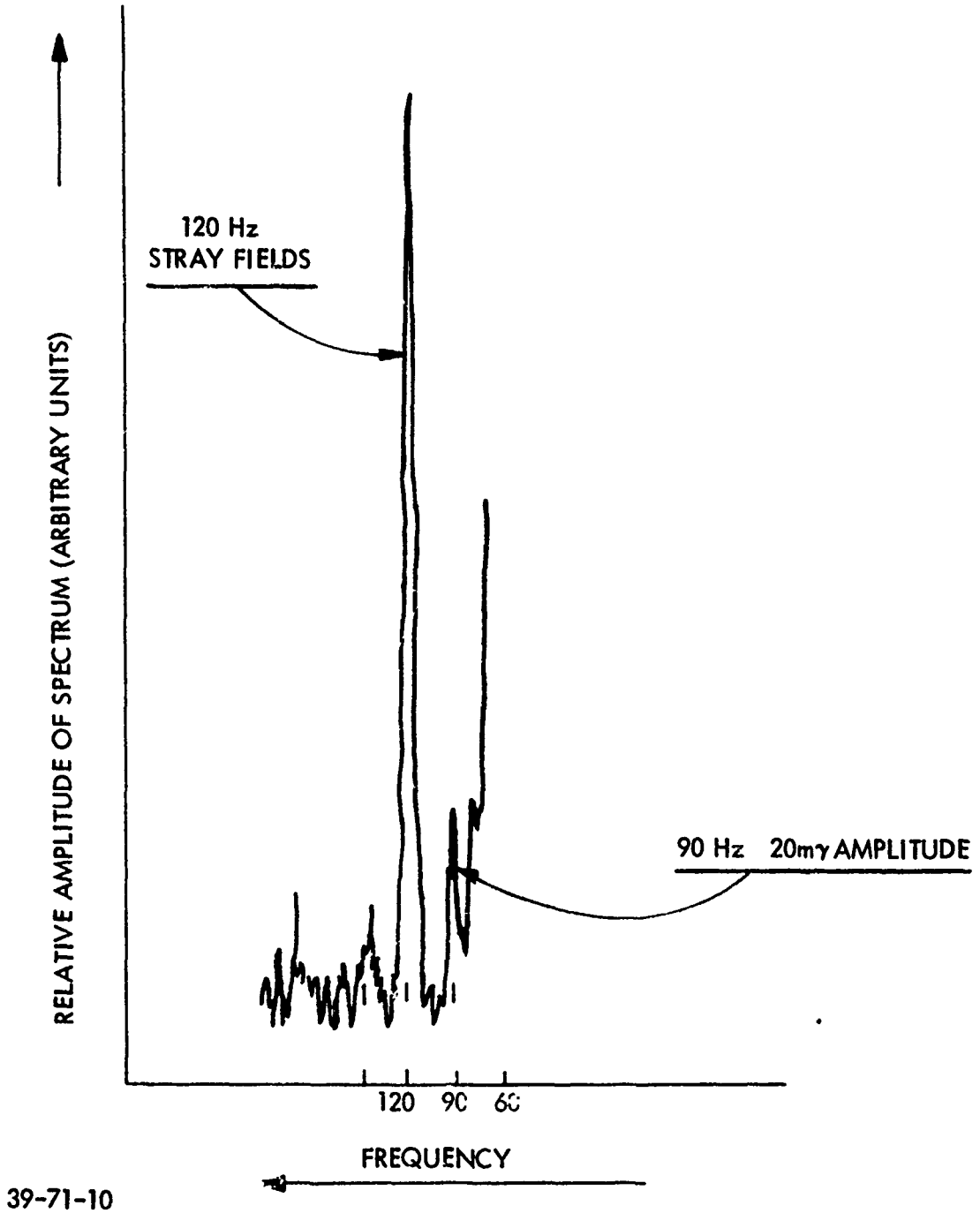

TRACING OF WAVE ANALYZER OUTPUT SHOWING PORTION OF SPECTRUM OF CESIUM MAGNETOMETER WITH 20 mγ 90 Hz SIGNAL PRESENT
FIGURE 6-1

SECTION VII

7.0 DISCUSSION OF THE RESULTS OF THE PROGRAM

As a result of the investigations carried out on this program, experimental techniques have been developed that allow the design of a gradient magnetometer with a differential sensitivity of 0.1 mγ (10^{-9} Gauss). The performance of resonance cells as measured by their signal-to-noise ratio and transverse relaxation time has been advanced to the level for achieving 0.1 mγ sensitivity as specified by the theory. The test operation of the unit as a single sensor cell magnetometer has experimentally demonstrated performance within an order of magnitude of the desired sensitivity and means are available for extrapolating this observed performance to the region of 0.1 mγ. The demonstration of this performance capability strengthens the validity of the theory for predicting magnetometer performance.

The experimental techniques that were developed for detection and amplification of the signals and for conducting the light beams are all compatible with the requirements for building a gradient, dual cell instrument.

SECTION VIII

8.0 TECHNOLOGICAL FORECAST

The work carried out on this program has established the experimental techniques for building gradient magnetometers with a higher sensitivity than has been possible up to now. The high sensitivity and airborne capability of this instrumentation will make it valuable in areas in which measurements of spatial or temporal variations in the earth's gradient field are desired, such as geophysical prospecting. The gradient device may also be useful in the area of search and surveillance.

The newly developed methods for improving the experimental parameters governing the resonances makes possible the application of these techniques to new technological areas. Areas of application which have previously been considered impractical because of low signal-to-noise and/or large-sized equipment should be re-examined. Some of these areas are in communications and signal processing particularly where conventional techniques appear to be at the limit of the state of the art.

In addition, the work performed on this program indicated that the values for the experimental parameters that were reached are not limits and with further investigation could be improved by orders of magnitude, thus offering further increases in sensitivity beyond the 0.1 mγ range. A value of 0.01 mγ appears extremely likely.

9. BIBLIOGRAPHY

1. Engineering in the Ocean Environment · Record IEEE Publication 72 CHO 660-1 OCC (Sept. 1972) p. 308.

2. Handbuch der Physik - Encyclopedia of Physics Vol. XLIX/3 K. Rawer, Ed. Springer-Verlag 1971, p. 430.

3. J.A. Jacobs, "Geomagnetic Micropulsations", Springer-Verlag 1970, p. 20.

4. E.H. Takken, "An Evaluation of Cryogenic and Competing Non-cryogenic Devices for Naval Applications Such as MAD, Surveillance, Radiation Detection, and Communications" (March 29, 1972), NRL Report 7400.

5. H.G. Dehmelt, Phys. Rev. 105, 1924 (1957).

6. J.H. Simpson and D.S. Bayley, "Research and Development Program on Optically Pumped Nuclear Magnetic Resonance", Final Report, GPL Report No. A-33-10, April 1968, (CONFIDENTIAL) Contract No. N00017-67-2419.

7. W.A. Edson, Proc. IRE, 48, 1454 (1960).

8. W. Happer, Rev. of Mod. Phys. 44, 169 (1972).

9. B. Cagnac, Ann. Phys. (Paris) 6, 467 (1961).

10. R.G. Brewer, Rev. Sci. Instr. 32, 1356 (1961).

11. F.A. Franz and E. Lüscher, Phys. Rev., 135, A582 (1964).

12. R.A. Bernheim, J. Chem. Phys. 36, 135 (1962).

13. M.A. Bouchiat and J. Brossel, Phys. Rev. 147, 147 (1966).

14. G. Singh, P. Delavore, and C.O. Alley, Rev. Sci. Inst. 43, 1388 (1972).

15. W.E. Bell and A.L. Bloom, Phys. Rev. 107, 1559 (1957).

16. J.L. Meilleroux, Rev. de Phys. Appl. 5, 121 (1970).

17. F. Bloch and A. Siegert, Phys. Rev. 57, 522 (1940).

18. H.Y. Carr and E.M. Purcell, 94, 630 (1954).

19. J.H. Simpson, "Interim Report on Nuclear Gyroscope", (March 1960) AD 318-124.